Supporting Information

Chemically Accurate Predictions for Water Adsorption on Brønsted Sites of Zeolite H-MFI

Henning Windeck,[a] Fabian Berger,[§][a] and Joachim Sauer*[a,b]

[a] Institut für Chemie, Humboldt-Universität zu Berlin, Unter den Linden 6, 10099 Berlin, Germany

E–Mail: js@chemie.hu-berlin.de

[b] Department of Physical and Macromolecular Chemistry and Charles University Centre of Advanced Materials, Charles University, 12843 Prague, Czech Republic

[§] Present address: Yusuf Hamied Department of Chemistry, University of Cambridge, CB2 1EW Cambridge, United Kingdom

Table of Contents

S1 Method Tests

S1.1 Influence of the Basis Set on Hybrid Optimisations

Because of the self–interaction error, PBE+D2 adsorption structures show a systematic underestimation of the strength of covalent bonds. To assess the severity of this error, reoptimisations are performed with the reliable MP2:PBE+D2 method. Two main parameters can be tuned for hybrid methods like MP2:PBE+D2: the basis set as well as the size and shape of the clusters used for high–level calculations. Further, the high–level method itself can be varied. While MP2:PBE+D2 has already proven to yield reliable structures in previous studies,[1-9] using hybrid DFT as in B3LYP+D3:PBE+D2 is an alternative with reduced computational cost. This section uses a small test set of water adsorption structures to evaluate which basis sets and cluster sizes are needed to obtain converged MP2:PBE+D2 and B3LYP+D3:PBE+D2 adsorption structures and to estimate the error for the chosen settings.

The test set consists of three adsorption structures at the Al11–O24(H)–Si10 site: (a) motif B for loading 1 H_2O/BAS (BAS = Si–O(H)–Al active site) with no deprotonation (*DoD = 0.15 ≈ 0*), (b) motif BH for loading 2 H_2O/BAS with half–deprotonation (*DoD =0.41 ≈ 0.5*), and (c) motif BHH for loading 3 H_2O/BAS with full deprotonation (*DoD = 0.96 ≈ 1*). Al11–O24(H)–Si10 is chosen because it features PBE+D2 water adsorption structures at these borderline cases of the *DoD*. For motif BH, a conformer is chosen that is slightly less stable (+6 kJ mol^{-1} with PBE+D2) than the most stable conformer. This is because it features a *DoD* of approx. 0.5, constituting a borderline case in the deprotonation of the BAS, which – at the PBE+D2 PES – is a stepless process. The three adsorption structures are presented in Figure S1.
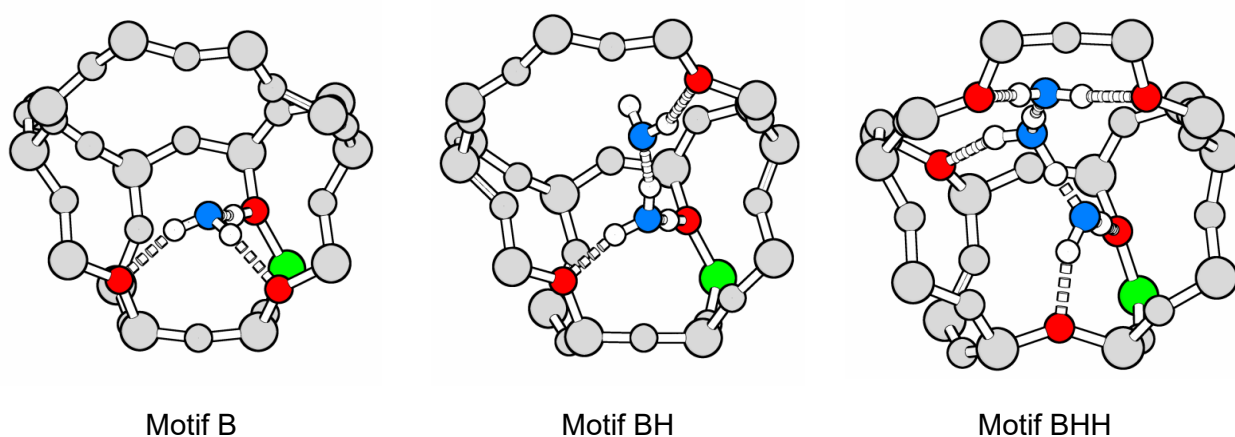

| Motif B | Motif BH | Motif BHH |

Figure S1: Representative set of water adsorption structures at the Brønsted acid site of Al11–O24(H)–Si10 (B, BH, and BHH). Colour code: aluminium – green, framework oxygen with hydrogen bond – red, oxygen in water molecules – blue, framework silicon and oxygen – grey, hydrogen – white.

To test the influence of the basis set on the adsorption structures and energies, hybrid MP2:PBE+D2 structure optimisations are performed with multiple basis sets from the Dunning and Ahlrichs families.[10-12] From each basis set family, a triple–zeta basis set (def2–TZVPP and cc–pVTZ), a triple–zeta basis set with diffuse functions (def2–TZVPPD and aug–cc–pVTZ), and a quadruple–zeta basis set (def2–QZVPP and cc–pVQZ) is used. Within this work, additional polarisation functions are standardly used for the Ahlrichs basis sets in high–level cluster calculations. For the high–level MP2 calculations, the smallest cluster consists of two corner–sharing TO_4 (T=Si/Al) tetrahedra that are connected via a bridging hydroxyl group – the 2T cluster. The 2T cluster is used for this test due to the high computational cost of canonical MP2 calculations at the quadruple-zeta basis set level. The influence of the cluster size is separately discussed in Section 1.2. Table S1 presents the basis set effect on the adsorption energies and the *DoD*. Table S2 presents differences in OH bond lengths.

Table S1: Adsorption energies E_{ads} in kJ mol^{-1} and degrees of deprotonation (*DoD*) based on optimisations with periodic PBE+D2 and reoptimisations with MP2:PBE+D2 using a 2T cluster and varying basis sets.

		B		BH		BHH	
		DoD	E_{ads}	*DoD*	E_{ads}	*DoD*	E_{ads}
PBE+D2	pbc	0.15	−97	0.41	−155	0.96	−234
MP2:PBE+D2	cc–pVTZ	0.07	−91	0.11	−142	0.97	−208
	aug–cc–pVTZ	0.07	−86	0.11	−133	0.98	−197
	cc–pVQZ	0.07	−87	0.11	−135	0.98	−200
	def2–TZVPP	0.07	−87	0.11	−134	0.98	−197
	def2–TZVPPD	0.07	−85	0.11	−131	0.98	−194
	def2–QVZPP	0.07	−84	0.10	−130	0.98	−194

With respect to the *DoD*, the adsorption structures are already converged for standard triple–zeta basis sets. Compared to benchmark results with def2-QZVPP, the mean absolute deviation (MAD) of all OH bond lengths is between 1.0–1.7 pm for cc–pVTZ and 0.5–0.6pm for def2–TZVPP. Thus, the def2–TZVPP basis set performs better than the analogous cc–pVTZ basis set. While the cc–pVnZ basis sets are hierarchical and basis functions are added systematically with every increase in the cardinal number n, the series of def2–nZVPP basis sets is not strictly hierarchical and the individual basis sets are optimised to yield the best results for a given basis set size.[10-18] Therefore, the def2–QZVPP basis set is considered the benchmark in this test. As a result, the def2–TZVPP basis set is used for all hybrid structure optimisations, because no basis set extrapolation is performed for these calculations.

Table S2: Mean absolute deviations (MAD(ΔR_{OH})) and maximum absolute deviations (MAX(ΔR_{OH})) of all OH bond lengths in pm and percent with respect to those obtained with the def2–QZVPP basis set as obtained by MP2:PBE+D2 reoptimisations (2T cluster).

		MAD(ΔR_{OH})		MAX(ΔR_{OH})	
		pm	%	pm	%
B	cc–pVTZ	1.0	0.5	3.5	1.7
	aug–cc–pVTZ	0.5	0.4	0.8	0.5
	cc–pVQZ	0.3	0.1	1.1	0.5
	def2-TZVPP	0.6	0.3	2.2	1.1
	def2-TZVPPD	0.4	0.3	0.8	0.5
	def2-QZVPP	0.0	0.0	0.0	0.0
BH	cc–pVTZ	1.7	0.9	6.8	3.1
	aug–cc–pVTZ	0.7	0.4	3.1	1.4
	cc–pVQZ	0.4	0.2	1.5	0.7
	def2-TZVPP	0.5	0.3	1.6	0.8
	def2-TZVPPD	0.5	0.3	1.4	0.9
	def2-QZVPP	0.0	0.0	0.0	0.0
BHH	cc–pVTZ	1.3	0.9	4.7	2.9
	aug–cc–pVTZ	0.4	0.3	0.8	0.8
	cc–pVQZ	0.2	0.1	0.6	0.4
	def2-TZVPP	0.6	0.5	2.8	1.7
	def2-TZVPPD	0.2	0.2	0.4	0.3
	def2-QZVPP	0.0	0.0	0.0	0.0

For the adsorption energies, however, the overall picture is different. With increasing basis set quality, the structures converge faster than the adsorption energies. Referenced to the benchmark results with def2–QZVPP, the adsorption energies obtained with the standard triple–zeta basis sets differ by 7 to 14 kJ mol^{-1} for cc–pVTZ and by only 3 to 4 kJ mol^{-1} for def2–TZVPP. Using augmented triple–zeta basis sets, the deviations range from 1 to 3 kJ mol^{-1} for aug–cc–pVTZ and 0 to 1 kJ mol^{-1} for def2–TZVPPD. This shows that augmentation enhances the results in a similar way than the transition to a higher cardinal number. Again, Ahlrich's basis sets show faster convergence. Therefore, they should be used whenever basis set extrapolation, which needs hierarchical basis sets like those of Dunning, is not possible.

S1.2 Influence of the Cluster Size on Hybrid Optimisations

Using the def2–TZVPP basis set in MP2 cluster calculations, MP2:PBE+D2 reoptimisations of PBE+D2 structures are performed with differently sized clusters to find out which cluster size is needed to obtain converged adsorption structures. Thereby, changes to the adsorption structures are directly assessed through the *DoD* and deviations in the OH bond lengths. Further, the influence of structural changes on the adsorption energies is probed with single–point calculations using a consistent methodology (MP2:PBE+D2 with benchmark cluster size). The minimal 2T cluster only captures the primary interaction of one water molecule with the BAS and interactions between the water molecules. Yet, the adsorbed water molecules have secondary hydrogen bonding interactions with framework oxygen atoms. Therefore, the minimal 2T cluster is enlarged stepwise until all secondary hydrogen bonds are incorporated. The enlargement steps are chosen such that closed rings of TO_4 (T = Si/Al) tetrahedra are formed, resulting in the succession: 2T, 6T, 12T, and 16T. The 16T cluster covers all secondary hydrogen bonds in all three adsorption structures. Therefore, MP2:PBE+D2 with the 16T cluster is considered the benchmark for structure optimisations. The succession of clusters is depicted in Figure S2 and the results are presented in Table S3.

Reoptimisation with hybrid methods introduces significant structural changes. The *DoD* obtained for B and BH is significantly higher with PBE+D2 as compared to the hybrid methods, i.e., the BAS is more deprotonated with PBE+D2. Referencing to MP2:PBE+D2 (16T cluster), it shrinks from 0.15 to 0.06 for B and from 0.41 to 0.10 for BH. This highlights that PBE+D2 seriously underestimates the strength of the covalent OH bond in the bridging hydroxyl group which drastically affects the adsorption structures, especially in ambiguous protonation states. Consequently, the interaction between BAS and water molecules is overestimated and deprotonation of the BAS is predicted to happen too soon. This could lead to a serious bias in commonly conducted PBE+D (D=D2/D3) molecular dynamics simulations for water adsorption in zeolites.[19-25] For BHH, on the other hand, changes in the *DoD* are small and the BAS is clearly deprotonated with all methods. This signifies that reoptimisation with hybrid methods like MP2:PBE+D2 is crucial in situations where the *DoD* is on the tipping point but less important for adsorption structures with distinct protonation states.

(a) Cluster 2T (25 atoms)

(b) Cluster 6T (46 atoms)

(c) Cluster 12T (76 atoms)

(d) Cluster 16T (97 atoms)
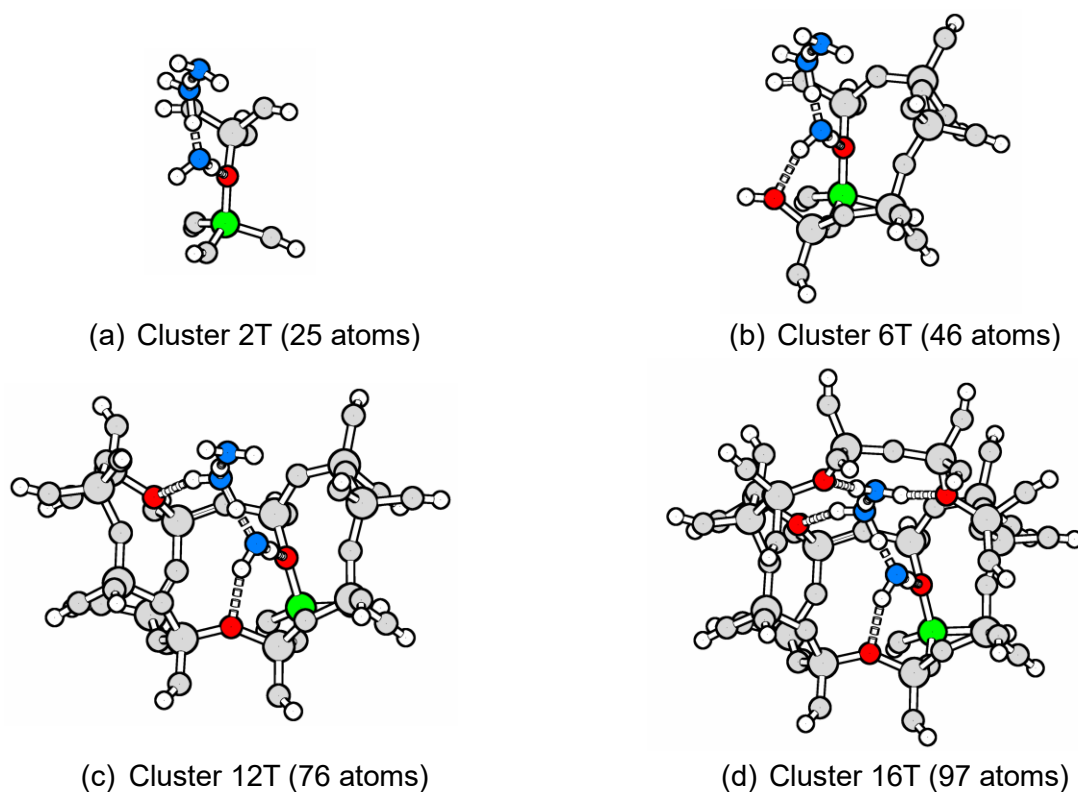
Figure S2: Clusters (2T, 6T, 12T, and 16T) shown for adsorption structure BHH at Al11–O24(H)–Si10. Colour code: aluminium – green, framework oxygen with hydrogen bond – red, oxygen in water molecules – blue, framework silicon and oxygen – grey, hydrogen – white.

The influence of structural changes on hybrid adsorption energies is probed by MP2:PBE+D2 single–point calculations with the 16T cluster which captures all hydrogen bonds. Comparing PBE+D2 (16T//0T) and MP2:PBE+D2 (16T//16T) optimised structures, total deviations of 1 kJ mol^{-1} for B, 3 kJ mol^{-1} for BH, and 2 kJ mol^{-1} for BHH are obtained. Given that these deviations are rather small, PBE+D2 optimisations can still be considered a reasonable approach. Nevertheless, PBE+D2 yields qualitatively different adsorption structures in some cases. Considering other sources of error as well, avoiding deviations of approximately 1–3 kJ mol^{-1} might be relevant to reach chemical accuracy (±4 kJ mol^{-1}). Hence, reoptimisation with hybrid methods is routinely applied in this work.

Table S3: Adsorption energies (E_{ads}) in kJ mol^{-1} and degrees of deprotonation (*DoD*) for B, BH, and BHH at Al11–O24(H)–Si10 as obtained by optimisations with periodic PBE+D2, B3LYP+D3:PBE+D2, and MP2:PBE+D2 using 2T, 6T, 12T, and 16T high–level clusters. DLPNO–MP2:PBE+D2 single–point calculations (16T high–level cluster) given for comparison. All high–level cluster calculations with def2–TZVPP basis set.

		B		BH		BHH	
		E_{ads}	*DoD*	E_{ads}	*DoD*	E_{ads}	*DoD*
PBE+D2	pbc	−96.8	0.15	−154.8	0.41	−233.7	0.96
	16T[a]//0T	−77.1	–	−116.3	–	−183.9	–
MP2:PBE+D2	2T//2T	−86.5	0.07	−134.0	0.11	−196.6	0.98
	16T[a]//2T	−77.0	–	−118.9	–	−182.4	–
	6T//6T	−77.8	0.07	−124.5	0.11	−191.5	0.97
	16T[a]//6T	−77.0	–	−118.9	–	−182.7	–
	12T//12T	−77.1	0.06	−123.6	0.10	−189.9	0.97
	16T[a]/12T	−76.7	–	−118.3	–	−182.1	–
	16T//16T	−77.7	0.06	−120.6	0.10	−184.3	0.97
	16T[a]//16T	−76.7	–	−118.8	–	−182.2	–
B3LYP+D3:PBE+D2	2T//2T	−90.3	0.08	−141.0	0.13	−207.2	0.98
	16T[a]//2T	−78.7	–	−120.7	–	−184.1	–
	6T//6T	−87.4	0.07	−139.7	0.12	−206.7	0.98
	16T[a]//6T	−77.2	–	−119.1	–	−182.6	–
	12T//12T	−89.1	0.07	−141.7	0.12	−210.8	0.98
	16T[a]/12T	−76.9	–	−118.8	–	−182.3	–
	16T//16T	−88.4	0.07	−140.9	0.12	−211.1	0.98
	16T[a]//16T	−76.7	–	−118.8	–	−182.2	–

[a]DLPNO–MP2:PBE+D2 single–point calculation (16T high–level cluster)

Reoptimisations with MP2:PBE+D2 and B3LYP+D3:PBE+D2 yield very similar structures. With respect to the *DoD,* the structures are already converged with the 2T cluster both for MP2:PBE+D2 and B3LYP+D3:PBE+D2. Deviations in OH bond lengths are reported in Table S4. Referenced to structures from MP2:PBE+D2 with the 16T cluster, MADs of the OH bond lengths of up to 1.7 pm are found for structures from MP2:PBE+D2 with the 2T cluster. The deviations decrease with increasing cluster size. The maximum deviations are 1.0 pm and 0.8 pm for 6T and 12T, respectively. Probing the influence of structural changes on the adsorption energies with DLPNO–MP2:PBE+D2 single–point calculations with the 16T cluster, slight improvements are seen for B3LYP+D3:PBE+D2 in the transition from 2T to 6T cluster, while changes are small for MP2:PBE+D2. Therefore, the 6T cluster is applied in all structure reoptimisations. The results suggest that B3LYP+D3:PBE+D2 yields reasonable structures at a significantly reduced computational cost.

Table S4: Mean absolute deviations (MAD(ΔR_{OH})) and maximum absolute deviations (MAX(ΔR_{OH})) of all OH bond lengths in pm and percent referenced to MP2:PBE+D2 with the 16T cluster for B, BH, and BHH at Al11–O24(H)–Si10 as obtained by reoptimisations with MP2:PBE+D2 and B3LYP+D3:PBE+D2 using 2T, 6T, 12T, and 16T high–level clusters. All high–level cluster calculations with def2–TZVPP basis set.

			MAD(ΔR_{OH})		MAX(ΔR_{OH})	
			pm	%	pm	%
B	PBE+D2	pbc	5.7	3.8	13.1	6.3
	MP2:PBE+D2	2T//2T	1.1	0.6	2.9	1.4
		6T//6T	0.9	0.5	3.1	1.5
		12T//12T	0.2	0.1	1.0	0.5
		16T//16T[a]	0.0	0.0	0.0	0.0
	B3LYP+D3:PBE+D2	2T//2T	1.5	0.8	3.8	1.8
		6T//6T	1.1	0.6	3.5	1.7
		12T//12T	0.8	0.4	2.6	1.2
		16T//16T	0.9	0.5	2.9	1.4
BH	PBE+D2	pbc	9.8	6.2	23.3	14.1
	MP2:PBE+D2	2T//2T	1.7	0.9	7.0	2.9
		6T//6T	1.0	0.5	3.5	1.4
		12T//12T	0.8	0.3	4.7	2.0
		16T//16T[a]	0.0	0.0	0.0	0.0
	B3LYP+D3:PBE+D2	2T//2T	1.9	1.0	8.5	3.8
		6T//6T	1.7	0.9	6.5	2.9
		12T//12T	1.7	0.9	7.7	3.5
		16T//16T	1.9	0.9	9.9	4.4
BHH	PBE+D2	pbc	2.1	1.6	5.6	3.6
	MP2:PBE+D2	2T//2T	1.4	0.8	4.5	2.4
		6T//6T	0.6	0.4	3.2	1.6
		12T//12T	0.5	0.3	3.3	1.6
		16T//16T[a]	0.0	0.0	0.0	0.0
	B3LYP+D3:PBE+D2	2T//2T	1.3	0.8	3.9	2.0
		6T//6T	1.0	0.6	4.3	2.2
		12T//12T	0.8	0.5	3.8	1.9
		16T//16T	0.5	0.3	1.9	0.9

[a]reference for calculation of MAD(ΔR_{OH}) and MAX(ΔR_{OH})

Since the structures obtained with differently sized clusters are very similar, the data presented in this section can also be used to assess the convergence of the adsorption energies with the cluster size. Referencing to the 16T cluster, significant deviations are found for the smaller clusters. While all secondary hydrogen bonding interactions are captured with the 6T cluster for B, they are only captured with the 16T cluster for BH and BHH. Convergence of the MP2:PBE+D2 adsorption energies with the cluster size occurs whenever this condition is met. For B, the deviation between the MP2:PBE+D2 adsorption energies obtained with the 6T and 12T clusters is <1 kJ mol^{-1}. For BH and BHH, however, it is 5 and 9 kJ mol^{-1}, respectively. Therefore, large clusters that capture all secondary hydrogen bonding interactions are used for the calculation of adsorption energies. The results obtained with B3LYP+D3:PBE+D2 are less sensitive towards the cluster size. This is because the B3LYP+D3:PBE+D2 energies are closer to PBE+D2 than the MP2:PBE+D2 energies

are. Thus, the differences are overall smaller, leading to smaller changes upon increasing the cluster size.

To evaluate the applicability of the DLPNO approximation, adsorption energies from MP2:PBE+D2 and DLPNO–MP2:PBE+D2 are compared for the 16T cluster. The deviations are 1.0 kJ mol^{-1} for B, 1.8 kJ mol^{-1} for BH, and 2.1 kJ mol^{-1} for BHH. These deviations are rather low but not insignificant. Yet, the DLPNO approximation allows for the use of sufficiently large clusters which is a prerequisite for accurate calculations. Due to the computational cost, canonical MP2:PBE+D2 with large clusters is only applicable to a few benchmark cases. Consequently, the DLPNO approximation is used for single–point energy calculations in this work.

Next, PBE+D2 adsorption energies are compared to adsorption energies from the hybrid methods that are converged with respect to the cluster size. Adsorption energies from PBE+D2 are more exoenergetic than those from MP2:PBE+D2 (16T cluster) by 20 kJ mol^{-1} for B, 18 kJ mol^{-1} per water molecule for BH, and 17 kJ mol^{-1} per water molecule for BHH. The corresponding results for B3LYP+D3:PBE+D2 are 11, 11, and 10 kJ mol^{-1}, respectively. For PBE+D2 and B3LYP+D3:PBE+D2, this can be considered a consequence of the self–interaction error, which leads to an overestimation of the hydrogen bonding interactions. Further, 2–body dispersion terms are described ab initio with MP2 while PBE+D2 and B3LYP+D3:PBE+D2 rely on approximate correction schemes.[26] The flaws of periodic PBE+D2 are only partially but not fully resolved by using hybrid DFT functionals like B3LYP. While B3LYP+D3:PBE+D2 is adequate for structure optimisations, it is insufficient for the calculation of chemically accurate adsorption energies.

Overall, the tests show that reoptimisation of PBE+D2 adsorption structures is needed. For structure optimisation, B3LYP+D3:PBE+D2 is nearly as reliable as MP2:PBE+D2. For the calculation of energies, B3LYP+D3:PBE+D2 does not reach MP2:PBE+D2 accuracy. Moreover, the structures converge much faster with basis set size and cluster model size than the energies.

S1.3   MP2:(PBE+D2)+ΔCC Adsorption Energies

While the settings obtained in the previous sections deliver converged adsorption structures, they do not yield converged adsorption energies. So far, the tests show that large clusters incorporating all secondary hydrogen bonds are needed to obtain MP2:PBE+D2 adsorption energies that are converged with respect to the cluster size. This section aims to establish a reliable protocol for the calculation of adsorption energies with MP2:(PBE+D2)+ΔCC for the water adsorption in H–MFI.

MP2 has methodical limitations that are assessed and remedied by calculating corrections with CCSD(T) (ΔCC). The DLPNO approximation is used both with MP2 and CCSD(T) in the single–point energy calculations discussed in this section. It is tested which cluster size suffices to obtain converged ΔCC corrections. Three differently sized clusters are used to calculate ΔCC corrections: 3T, 6T, and 12T, see Figure S2. The 6T cluster is equivalent to the cluster used in the MP2:PBE+D2 reoptimisations of the structures. The results are presented in Table S5.

Table S5: Cluster–only MP2 and CCSD(T) adsorption energies (E_{ads}) and CCSD(T) corrections (ΔCC) in kJ mol^{-1} for B, BH, and BHH at Al11–O24(H)–Si10 (MP2:PBE+D2 reoptimised structures). E_{ads} given total and divided by number of water molecules. All high–level cluster calculations with cc–pVTZ basis set.

		B	BH		BHH	
		total	total	per H$_2$O	total	per H$_2$O
3T	MP2	−132.7	−128.5	−64.2	−127.2	−42.4
	CCSD(T)	−130.5	−124.9	−62.5	−117.2	−39.1
	ΔCC	2.2	3.6	1.8	10.0	3.3
6T	MP2	−70.6	−101.5	−50.8	−99.4	−33.1
	CCSD(T)	−66.8	−95.6	−47.8	−87.7	−29.2
	ΔCC	3.9	5.9	3.0	11.8	3.9
12T	MP2	−72.5	−101.9	−51.0	−122.5	−40.8
	CCSD(T)	−69.4	−96.6	−48.3	−111.2	−37.1
	ΔCC	3.1	5.3	2.6	11.3	3.8

All obtained ΔCC corrections are positive which means that MP2 slightly overestimates the strength of the interaction. Throughout the test, ΔCC per water molecule is found to be rather constant and lies between 2–4 kJ mol^{-1}. Regarding ΔCC, the results obtained with the 6T and 12T clusters deviate by less than 1 kJ mol^{-1} in all three cases. Therefore, the 6T cluster is employed in all calculations of ΔCC. The 3T cluster is not used because it yields an adsorption energy for B that is 62 kJ mol^{-1} more exoenergetic than the converged adsorption energy obtained with the 6T and 12T clusters. Further, deviations in ΔCC are higher for the 3T cluster with up to 2 kJ mol^{-1}. Comparing B with BH and BHH, the 3T cluster predicts decreasing total adsorption energies which is at variance with the results obtained for the larger clusters. This can be explained by the fact that the 3T cluster captures only the primary interaction of one water molecule with the active site but neglects the secondary hydrogen bonding interactions which stabilise additional water molecules in their respective adsorption structures. For the same reason, the total adsorption energy decreases from BH to BHH for the 6T cluster. In this work, ΔCC corrections are only calculated for the loadings 1 H$_2$O/BAS and 2 H$_2$O/BAS because these are borderline cases with respect to the deprotonation of the BAS. Hence, the 6T cluster suffices to obtain accurate results.

In the investigation of adsorption processes, the basis set superposition error (BSSE) plays an important role. The BSSE is corrected with the Counterpoise (CP) correction.[27] With increasing water

loading, the BAS is eventually deprotonated. In such adsorption structures, the proton that formerly belonged to the BAS is now part of a positively charged water cluster. This situation introduces ambiguity in the fragment selection for the CP correction. For example, the Zundel ion ($H_5O_2^+$) constitutes such a case, see Figure S3.
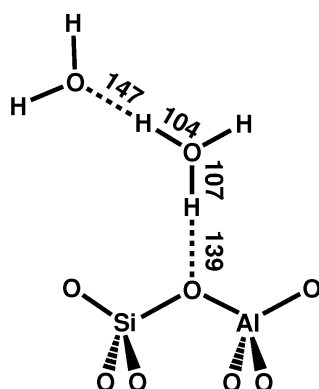

Figure S3: Schematic representation of a Zundel ion ($H_5O_2^+$) at Al11–O24(H)–Si10 with bond lengths in pm.

In the chemical picture, the unperturbed acidic zeolite (ZOH) reacts with two unperturbed water molecules (H_2O). While this seems to be an intuitive choice for the monomers in the CP correction scheme, the obtained monomers are far from their equilibrium structures and feature OH bonds that are far from their equilibrium distances. Regarding only the adsorption structure, the monomers can be selected such that they constitute reasonable chemical moieties. To assess the influence of different monomer selections for the CP correction, sensible selections are tested for adsorption motif BH at Al11–O24(H)–Si10, see Table S6.

Table S6: MP2:(PBE+D2)+ΔCC adsorption energies for BH at Al11–O24(H)–Si10 (most stable conformer, *DoD* = 0.82) in kJ mol^{-1} using the MP2:PBE+D2 adsorption structure. Extrapolation to complete basis set limit (CBS) with cc–pVTZ and cc–pVQZ basis sets. Counterpoise (CP) correction with different monomer selections.

		cc–pVTZ	cc–pVQZ	CBS cc–pVnZ (n = T,Q)
Not CP–corrected	–	−121.8	−106.5	−103.1
CP–corrected	ZOH + H_4O_2	−94.9	−105.9	−116.2
	ZOH + H_2O + H_2O	−92.1	−106.9	−119.2
	ZO$^-$ + $H_5O_2^+$	−100.0	−101.5	−107.2
	ZO$^-$ + H_3O^+ + H_2O	−95.7	−103.0	−111.6
	ZO$^-$ + H_2O + H_3O^+	−90.8	−102.4	−113.5

For the cc–pVTZ and cc–pVQZ basis sets, the adsorption is most exoenergetic if no CP correction is used. This is most pronounced for the cc–pVTZ basis set because the BSSE decays with increasing basis set size. This trend is reversed for the values obtained from basis set extrapolation. While the adsorption energies decrease (in absolute terms) from cc–pVTZ to cc–pVQZ for the non–corrected values, those obtained with the CP correction increase. Thus, the CP correction is particularly needed for calculations with cc–pVTZ to obtain reliable results from basis set extrapolation. After basis set extrapolation, the adsorption energy without CP correction is −103 kJ mol^{-1} while the CP–corrected values range from −107 to −119 kJ mol^{-1}.

The choice of fragments for the CP correction has a significant impact on the adsorption energies. First, the water cluster can either be used as one fragment or split up further. If it is not split up, the BSSE that arises from the formation of the water cluster is not corrected. Nevertheless, this approach could be necessary if the wavefunctions of the separated parts would deviate too much from the original wavefunction – a limitation of the CP correction. This could particularly be the case for the free Zundel ion in which the proton sits exactly in the middle between two water molecules.[28] There, any possible choice of fragments would lead to OH bonds that are far from their equilibrium distances. Fortunately, the interaction of the Zundel ion with the zeolite leads to a clearer picture. To test the influence of different monomer selections on the adsorption energies, $ZO^-+H_5O_2^+$ is split into $ZO^-+H_3O^++H_2O$ and $ZO^-+H_2O+H_3O^+$. Thereby, the additional proton is attributed to one water molecule in the former and to the other water molecule in the latter case. The fact that $ZO^-+H_3O^++H_2O$ and $ZO^-+H_2O+H_3O^+$ yield results that differ by only 1.9 kJ mol^{-1} after basis set extrapolation justifies the approach of splitting the water cluster into fragments.

Secondly, the additional proton can either be attributed to the BAS – to which it is bonded in the bare system – or to the water cluster. Although the BAS is deprotonated in the case of Zundel ion formation, the additional proton is still attributed to it in the case of $ZOH+H_4O_2$ and $ZOH+H_2O+H_2O$. This results in a large distance between the bridging oxygen atom and the proton, see Figure S3, which is far from the equilibrium distance and leads to deviations in the adsorption energy of up to 5.7 kJ mol^{-1} compared to $ZO^-+H_3O^++H_2O$. Consequently, close attention must be paid to a physically sound choice of fragments for the CP correction.

In sum, the tests presented in this section yield accurate settings for the MP2:(PBE+D2)+ΔCC single–point energy calculations used in this work. The corrections ΔCC are calculated for the same clusters that are used in MP2:PBE+D2 structure reoptimisations (6T clusters). Basis set extrapolation with the cc–pVnZ (n = T,Q) basis sets is employed. The magnitude of the CP correction varies vastly with the choice of fragments which thus must be chosen using chemical intuition.

An error estimation for the introduced MP2:(PBE+D2)+ΔCC method can be approached using the insights obtained from all method tests. Structure optimisation with MP2:PBE+D2 is converged with the def2–TZVPP basis set and the chosen cluster size. With the chosen cluster size, ΔCC shows maximum deviations of 0.8 kJ mol^{-1} per adsorbed water molecule to the results obtained with the benchmark cluster size. The DLPNO approximation introduces errors below 0.9 kJ mol^{-1} per adsorbed water molecule. The error that arises from the basis set incompleteness error is minimised for the final values by basis set extrapolation. For the CP correction, a conservative estimate for the error that arises from different monomer choices is the difference in the adsorption energies between $ZO^-+H_3O^++H_2O$ and $ZO^-+H_2O+H_3O^+$. It amounts to 1.0 kJ mol^{-1} per water molecule. The Euclidian norm of all quantifiable errors in the MP2:(PBE+D2)+ΔCC benchmark electronic energies is 1.6 kJ mol^{-1} per adsorbed water molecule. Yet, this does not include errors in the zero–point vibrational energies and thermal contributions which are based on periodic PBE+D2.

S1.4 Conformer Selection

For each adsorption motif at every framework position, multiple different adsorption structures (conformers) exist due to the formation of secondary hydrogen bonds. Calculating high–level corrections (ΔMP2 and ΔCC) for every conformer, however, is not feasible. Thus, we select the most stable conformer at the PBE+D2 level for the calculation of high–level corrections (results in Table 2 of the main text). Assuming similar high–level corrections for the different conformers, the high–level corrections would not affect the stability order of the conformers, i.e. PBE+D2 would correctly predict the most stable conformer. We test this hypothesis by calculating high–level corrections for all conformers of B, L, and BH at framework position Al2–O7(H)–Si6. Table S7–S9 show the results.

Table S7: Degrees of deprotonation (*DoD*), adsorption energies (E_{ads}), high–level corrections (ΔMP2, ΔCC), adsorption enthalpies at 298 K (H_{ads}), zero–point energy contributions (ΔZPVE), and thermal enthalpy contributions at 298 K ($\Delta H_{0K \to 298K}$) in kJ mol^{-1} as obtained with PBE+D2 and MP2:(PBE+D2)+ΔCC for all conformers (conf.) of B at Al2–O7(H)–Si6.

conf.	PBE+D2					MP2:(PBE+D2)+ΔCC				
	DoD	E_{ads}	H_{ads}	ΔZPVE	$\Delta H_{0K \to 298K}$	*DoD*	E_{ads}	H_{ads}[a]	ΔMP2	ΔCC
1[b]	0.07	−69.7	−63.2	9.2	−2.7	0.04	−63.7	−57.1	5.1	−1.0
2	0.07	−69.1	−63.3	7.8	−2.0	0.04	−63.9	−58.1	4.8	−1.0
3	0.09	−68.8	−62.6	8.7	−2.4	0.05	−62.2	−56.0	6.5	−1.1
4	0.07	−68.1	−62.0	7.6	−1.5	0.03	−62.9	−56.8	4.8	−1.2
5	0.10	−66.1	−60.6	8.5	−3.0	0.04	−57.7	−52.2	8.0	−1.7
6	0.10	−66.1	−60.9	7.7	−2.5	0.04	−57.8	−52.6	8.0	−1.8
7	0.08	−65.2	−59.0	8.3	−2.2	0.04	−57.5	−51.4	8.1	−1.7
8	0.09	−65.0	−59.1	8.3	−2.4	0.04	−58.7	−52.8	5.8	−1.3
9	0.06	−63.1	−56.8	7.7	−1.4	0.03	−57.0	−50.7	6.4	−1.4

[a]ΔZPVE and $\Delta H_{0K \to 298K}$ from PBE+D2; [b]Originally chosen for calculation of high–level corrections, see Table 2 in main text

Table S8: Adsorption energies (E_{ads}), high–level corrections (ΔMP2, ΔCC), adsorption enthalpies at 298 K (H_{ads}), zero–point energy contributions (ΔZPVE), and thermal enthalpy contributions at 298 K ($\Delta H_{0K \to 298K}$) in kJ mol^{-1} as obtained with PBE+D2 and MP2:(PBE+D2)+ΔCC for all conformers (conf.) of L at Al2–O7(H)–Si6.

conf.	PBE+D2				MP2:(PBE+D2)+ΔCC			
	E_{ads}	H_{ads}	ΔZPVE	$\Delta H_{0K \to 298K}$	E_{ads}	H_{ads}[a]	ΔMP2	ΔCC
1[b]	−69.9	−62.6	11.2	−3.8	−67.0	−59.6	3.5	−1.3
2	−69.9	−62.6	11.2	−3.8	−66.9	−59.5	3.6	−1.3
3	−69.7	−62.7	10.7	−3.7	−66.3	−59.3	4.0	−1.2
4	−65.5	−57.8	11.4	−3.7	−58.6	−50.9	7.7	−1.3
5	−63.8	−56.8	10.1	−3.0	−58.7	−51.6	5.8	−1.1
6	−44.4	−37.2	9.6	−2.5	−42.0	−34.9	5.2	−3.2

[a]ΔZPVE and $\Delta H_{0K \to 298K}$ from PBE+D2; [b]Originally chosen for calculation of high–level corrections, see Table 2 in main text

Table S9: Degrees of deprotonation (*DoD*), adsorption energies (E_{ads}), high–level corrections (ΔMP2, ΔCC), adsorption enthalpies at 298 K (H_{ads}), zero–point energy contributions (ΔZPVE), and thermal enthalpy contributions at 298 K ($\Delta H_{0K \to 298K}$) in kJ mol^{-1} as obtained with PBE+D2 and MP2:(PBE+D2)+ΔCC for all conformers (conf.) of BH at Al2–O7(H)–Si6.

conf.	PBE+D2					MP2:(PBE+D2)+ΔCC				
	DoD	E_{ads}	H_{ads}	ΔZPVE	$\Delta H_{0K \to 298K}$	*DoD*	E_{ads}	$H_{ads}{}^{a}$	ΔMP2	ΔCC
1[b]	0.94	−162.2	−155.1	15.9	−8.7	0.92	−123.2	−116.0	34.2	3.1
2	0.93	−161.4	−151.5	18.5	−8.6	0.93	−131.5	−121.6	26.2	1.5
3	0.93	−161.3	−151.5	18.2	−8.3	0.93	−131.5	−121.6	26.2	1.5
4	0.91	−156.7	−146.9	17.9	−8.0	0.84	−122.8	−112.9	28.3	2.6
5	0.87	−156.6	−147.2	17.4	−8.0	0.85	−123.3	−113.9	28.4	2.7
6	0.93	−153.4	−146.2	15.9	−8.6	0.89	−113.7	−106.5	35.0	2.5
7	0.90	−141.1	−133.3	15.9	−8.1	0.89	−110.4	−102.6	26.9	2.0
8	0.88	−141.1	−133.4	15.7	−8.1	0.87	−111.3	−103.7	26.3	1.8
9	0.58	−140.7	−135.4	11.8	−6.5	0.14	−125.4	−120.1	17.9	−0.4
10	0.95	−135.8	−126.5	17.4	−8.1	0.96	−106.6	−97.3	25.6	2.0
11	0.87	−130.7	−121.7	17.3	−8.3	0.88	−96.8	−87.8	30.4	2.0

$^{a}\Delta$ZPVE and $\Delta H_{0K \to 298K}$ from PBE+D2; ^{b}Originally chosen for calculation of high–level corrections, see Table 2 in main text

For adsorption motif B, the ΔMP2 and ΔCC corrections range from 4.8 to 8.1 kJ mol^{-1} and −1.0 to −1.8 kJ mol^{-1}, respectively. This small variation in the ΔMP2 and ΔCC corrections does not lead to significant changes in the stability order within the set of conformers, justifying our assumption. The overall picture for adsorption motif L is very similar, with ΔMP2 and ΔCC corrections ranging from 3.5 to 7.7 kJ mol^{-1} and −1.1 to −3.2 kJ mol^{-1}, respectively. As before, these high–level corrections do not significantly alter the stability order of the conformers.

In contrast to the results for adsorption motifs B and L, the high–level corrections change the stability order for adsorption motif BH. We calculate ΔMP2 and ΔCC corrections in the range of 17.9 to 35.0 kJ mol^{-1} and −0.4 to 3.1 kJ mol^{-1}, respectively. The ΔMP2 corrections are large and vary significantly with the conformer, causing changes in the stability order of the conformers. While conformer 1 is 0.8 kJ mol^{-1} more stable than conformer 2 with PBE+D2, conformer 1 is 8.3 kJ mol^{-1} less stable than conformer 2 with MP2:(PBE+D2)+ΔCC. Figure S4 presents the structures of conformers 1, 2, and 9. These results challenge our assumption that PBE+D2 correctly predicts the most stable conformer. More importantly, it shows that PBE+D2 can even fail for the sampling of adsorption structures, challenging common practice in computational catalysis.
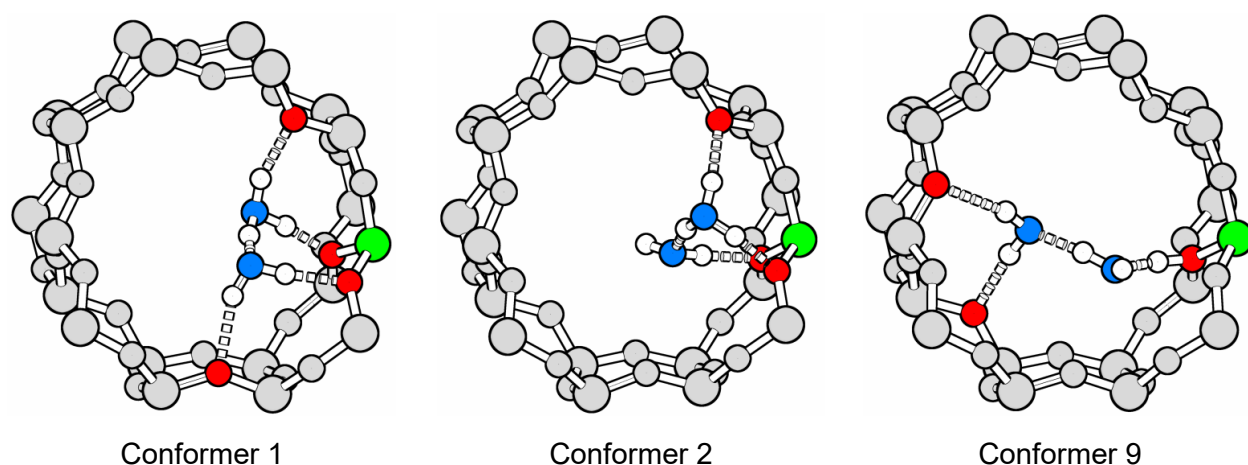
Conformer 1   Conformer 2   Conformer 9

Figure S4: Water adsorption structures of adsorption motif BH at framework position Al2–O7(H)–Si6. Conformers 1, 2, and 9 as presented in Table S9. Colour code: aluminium – green, framework oxygen with hydrogen bond – red, oxygen in water molecules – blue, framework silicon and oxygen – grey, hydrogen – white.

As predicted by PBE+D2, for adsorption motif BH at all framework positions, the respective most stable conformers feature a deprotonated BAS and a Zundel–ion–like water cluster (ionic adsorption), see Table 2 of the main text. The results from Table S9, however, suggest that PBE+D2 largely overestimates the stability of such Zundel–ion–like adsorption structures. Regarding less stable conformers as well, PBE+D2 yields multiple adsorption structures with ambiguous protonation states, i.e. 0.1<DoD<0.9. Multiple experimental and theoretical studies have examined at which loading the BAS is deprotonated and a stable protonated water cluster forms.[19, 29, 30] Generally, it is believed that a loading of 3 H_2O/BAS is required to deprotonate the BAS.[30] As a test, we calculate high–level corrections for the BH conformers with the lowest DoD (molecular adsorption) – in addition to the most stable ones presented in Table 2 of the main text. Tables S10–S12 present the results.

Table S10: Adsorption energies (E_{ads}) in kJ mol^{-1} and degrees of deprotonation (DoD) as obtained with PBE+D2 and MP2:(PBE+D2)+ΔCC for ionic (ZO^{-}···$H_5O_2^+$) and molecular (ZOH···H_4O_2) water adsorption in adsorption motif BH.

	PBE+D2				MP2:(PBE+D2)+ΔCC			
	E_{ads}		DoD		E_{ads}		DoD	
	ZO^{-} $H_5O_2^+$	ZOH H_4O_2	ZO^{-} $H_5O_2^+$	ZOH H_4O_2	ZO^{-} $H_5O_2^+$	ZOH H_4O_2	ZO^{-} $H_5O_2^+$	ZOH H_4O_2
Al2–O7(H)–Si6	−162.2	−140.7	0.95	0.58	−123.2	−125.4	0.92	0.14
Al3–O5(H)–Si2	−176.6	−168.2	0.94	0.48	−139.3	−136.7	0.92	0.19
Al6–O10(H)–Si3	−162.6	−141.0	0.92	0.37	−124.4	−120.6	0.91	0.14
Al7–O17(H)–Si18	−172.3	−162.2	0.89	0.67	−128.4	−134.3	0.88	0.21
Al11–O24(H)–Si10	−161.7	−138.0	0.82	0.27	−111.6	−112.6	0.82	0.08
Al12–O8(H)–Si3	−182.2	−161.2	0.92	0.30	−136.3	−133.2	0.91	0.14

Table S11: Contributions to the MP2:(PBE+D2)+ΔCC energies presented in Table S10, namely PBE+D2 energies on the MP2:PBE+D2 structures (E_{ads}), MP2 corrections (ΔMP2), and CCSD(T) corrections (ΔCC) in kJ mol^{-1} for ionic (ZO$^-$···H$_5$O$_2$$^+$) and molecular (ZOH···H$_4O_2$) water adsorption in adsorption motif BH.

	E_{ads}(PBE+D2//MP2:PBE+D2)[a]		ΔMP2		ΔCC	
	ZO$^-$ H$_5$O$_2$$^+$	ZOH H$_4$O$_2$	ZO$^-$ H$_5$O$_2$$^+$	ZOH H$_4$O$_2$	ZO$^-$ H$_5$O$_2$$^+$	ZOH H$_4$O$_2$
Al2–O7(H)–Si6	−160.5	−142.9	34.2	17.9	3.1	−0.4
Al3–O5(H)–Si2	−175.5	−165.1	33.0	26.6	3.2	1.8
Al6–O10(H)–Si3	−160.9	−137.6	34.4	16.4	2.1	0.6
Al7–O17(H)–Si18	−170.6	−157.8	36.0	20.5	6.2	2.9
Al11–O24(H)–Si10	−160.0	−132.2	42.5	18.0	5.9	1.6
Al12–O8(H)–Si3	−180.1	−158.3	39.2	23.5	4.6	1.7

[a]MP2:PBE+D2 structure

Table S12: Zero–point energy contributions (ΔZPVE), thermal enthalpy contributions at 298 K ($\Delta H_{\text{0K}\rightarrow\text{298K}}$), and adsorption enthalpies at 298 K (H_{ads}) in kJ mol^{-1} for ionic (ZO$^-$···H$_5$O$_2$$^+$) and molecular (ZOH···H$_4O_2$) water adsorption in adsorption motif BH. See Table S10 for the corresponding electronic adsorption energies.

	PBE+D2						MP2:(PBE+D2)+ΔCC	
	ΔZPVE		$\Delta H_{\text{0K}\rightarrow\text{298K}}$		H_{ads}		H_{ads}[a]	
	ZO$^-$ H$_5$O$_2$$^+$	ZOH H$_4$O$_2$	ZO$^-$ H$_5$O$_2$$^+$	ZOH H$_4$O$_2$	ZO$^-$ H$_5$O$_2$$^+$	ZOH H$_4$O$_2$	ZO$^-$ H$_5$O$_2$$^+$	ZOH H$_4$O$_2$
Al2–O7(H)–Si6	15.9	11.8	−8.7	−6.5	−155.1	−135.4	−116.0	−120.1
Al3–O5(H)–Si2	20.7	10.5	−10.1	−6.6	−165.9	−164.3	−128.6	−132.7
Al6–O10(H)–Si3	16.1	13.9	−8.1	−6.5	−154.5	−133.7	−116.4	−113.3
Al7–O17(H)–Si18	12.2	11.2	−8.8	−6.9	−168.9	−157.9	−125.0	−130.0
Al11–O24(H)–Si10	15.1	14.3	−8.7	−7.3	−155.3	−131.0	−105.3	−105.6
Al12–O8(H)–Si3	20.6	14.1	−10.8	−7.7	−172.4	−154.7	−126.5	−126.7

[a]ΔZPVE and $\Delta H_{\text{0K}\rightarrow\text{298K}}$ from PBE+D2

PBE+D2 strongly favours ionic over molecular water adsorption for all framework positions, with marked stability differences between 8.4 and 23.6 kJ mol^{-1}, see Table S10. It is noteworthy, however, that PBE+D2 does not yield any clear–cut cases of molecular adsorption but conformers with ambiguous protonation states of the BAS (0.1<DoD<0.9). These transform into clear–cut cases of molecular water adsorption through MP2:PBE+D2 structure optimisation, demonstrating that ambiguous protonation states are a PBE+D2 artifact. Figure 6 in the main text shows the PBE+D2 and MP2:PBE+D2 structures for Al7–O17(H)–Si18.

In contrast to PBE+D2, the benchmark MP2:(PBE+D2)+ΔCC results suggest similar stability of ionic and molecular adsorption structures, with stability differences between 1.0 and 6.0 kJ mol^{-1}. For MP2:(PBE+D2)+ΔCC, molecular adsorption is even favoured at three framework positions, agreeing well with experimental and theoretical studies stating that full deprotonation of the BAS only happens at loading 3 H$_2$O/BAS.[19, 29, 30] The ΔMP2 corrections are much larger for ionic than for molecular adsorption, eroding the marked stability differences predicted by PBE+D2, see Table S11. The ΔCC corrections behave similarly, yet on a much smaller scale. This highlights that PBE+D2 overestimates the stability of Zundel–ion–like, ionic adsorption structures. Considering the revealed limitations of PBE+D2, we show a need for more accurate yet computationally efficient sampling methods – a goal for future research.

S1.5 PBE+D2 vs. CCSD(T) for Cyclic Water Clusters

Tschumper and co–workers[31] calculate benchmark CCSD(T) interaction energies for the water clusters $(H_2O)_n$ with n=3–5. We calculate PBE+D2 interaction energies for these water clusters to assess the performance of PBE+D2 for such strongly H–bonded systems. They serve as a simple model for the complex situation of water clusters in zeolite pores. Table S13 presents the results. PBE+D2 severely overestimates the interaction strengths, i.e. the H–bond strengths, with deviations to the CCSD(T) reference of 23.0, 38.9, and 49.0 kJ mol^{-1} for $(H_2O)_3$, $(H_2O)_4$, and $(H_2O)_5$, respectively. Divided by the respective number of water molecules, we observe deviations between 7.7 and 9.8 kJ mol^{-1}. Further, the covalent O–H bond lengths for the H–bonded OH groups are significantly longer with PBE+D2 than with CCSD(T), with deviations ranging from 2.0 to 2.8 pm. These results demonstrate a general need to go beyond PBE+D2 for strongly H–bonded systems like water clusters.

Table S13: PBE+D2 and CCSD(T) interaction energies (E_{int}) and their differences (ΔE_{int}) in kJ mol^{-1}, as well as covalent O–H bond lengths (R_{OH}) in pm. PBE+D2 results with def2–TZVPP basis set. CCSD(T) benchmark results taken from ref. [31].

| | E_{int} | | ΔE_{int}(CCSD(T)−PBE+D2) | | R_{OH} | |
	PBE+D2	CCSD(T)[a]	total	per H_2O	PBE+D2	CCSD(T)[a]
$(H_2O)_3$	−89.0	−66.0	−23.0	−7.7	99.1	97.1
$(H_2O)_4$	−153.8	−114.9	−38.9	−9.7	100.4	97.7
$(H_2O)_5$	−199.8	−150.8	−49.0	−9.8	100.6	97.8

[a]see ref. [31]

S1.6 PBE+D2 vs. revPBE+D2/D3 for Adsorption Energies and Structures

For modelling of water, revPBE+D3 is claimed to perform well.[32] We test this for a selection of water adsorption structures at Al12–O(H)–Si3, see Tables S14–S17 for the results. Within the test set of structures, revPBE+D2 and revPBE+D3 differ by 1.4 to 5.8 kJ mol^{-1}. In comparison to PBE+D2 and the benchmark MP2:(PBE+D2)+ΔCC results, however, they yield the same qualitative trends.

Overall, revPBE+D2/D3 significantly improves over PBE+D2, yielding adsorption energies that are much closer to the MP2:(PBE+D2)+ΔCC benchmark. Yet, this improvement is not consistent for all interaction motifs. For some cases, revPBE+D2/D3 agrees well with MP2:(PBE+D2)+ΔCC, e.g. B and BL. For other cases, however, large deviations to MP2:(PBE+D2)+ΔCC are observed – up to 22.6 or 19.7 kJ mol^{-1} for revPBE+D2 and revPBE+D3, respectively. PBE+D2 consistently overestimates the binding energies, whereas revPBE+D2/D3 yield smaller deviations, but sometimes slightly larger and sometimes significantly smaller binding energies. As for the structures, revPBE+D2/D3 is often closer to the benchmark MP2:PBE+D2 structures than PBE+D2. This applies for both the H–bond lengths and the degrees of deprotonation.

Table S14: Adsorption energies for water adsorption at Al12–O(H)–Si3 in kJ mol^{-1} and their mean absolute deviations (MAD) with respect to MP2:(PBE+D2)+ΔCC. Loadings 1–3 H_2O/BAS with Brønsted–type (B) and Lewis–type (L) approach to the active site.

	MP2:(PBE+D2)+ΔCC	revPBE+D3	revPBE+D2	PBE+D2
B	−78.9	−82.1	−83.5	−93.5
L	−44.7	−36.1	−40.5	−54.8
BH – ion-pair complex	−136.3	−153.7	−158.9	−182.2
BH – neutral complex	−133.2	−143.3	−144.3	−161.2
BL	−108.5	−103.1	−109.0	−130.0
BHH	−207.0	−226.7	−229.2	−259.3
BHL	−176.6	−180.8	−183.7	−214.7
MAD	reference	9.8	10.3	30.1

Table S15: Differences of adsorption energies with respect to the MP2:(PBE+D2)+ΔCC energies for water adsorption at Al12–O(H)–Si3 in kJ mol^{-1}. Loadings 1–3 H_2O/BAS with Brønsted–type (B) and Lewis–type (L) approach to the active site.

	revPBE+D3	revPBE+D2	PBE+D2
B	−3.2	−4.6	−14.6
L	8.6	4.2	−10.1
BH – ion-pair complex	−17.4	−22.6	−45.9
BH – neutral complex	−10.1	−11.1	−28.0
BL	5.4	−0.5	−21.5
BHH	−19.7	−22.2	−52.3
BHL	−4.2	−7.1	−38.1

Table S16: H–bond lengths (ZOH···OH$_2$ or ZO$^-$···HOH$_2^+$, depending on protonation state) in pm and their mean absolute deviations (MAD) with respect to MP2:PBE+D2 for water adsorption structures at Al12–O(H)–Si3. Loadings 1–3 H_2O/BAS with Brønsted–type (B) and Lewis–type (L) approach to the active site.

	MP2:PBE+D2	revPBE+D3	revPBE+D2	PBE+D2
B	150.8	150.4	148.4	142.2
L	–	–	–	–
BH – ion-pair complex	151.5	153.7	158.7	158.0
BH – neutral complex	145.1	140.7	139.3	133.2
BL	161.4	161.1	160.4	152.2
BHH	149.6	153.0	154.3	153.9
BHL	148.3	144.0	144.3	136.9
MAD	reference	2.5	4.2	8.7

Table S17: Degree of deprotonation (DoD) and their mean absolute deviations (MAD) with respect to MP2:PBE+D2 for water adsorption structures at Al12–O(H)–Si3. Loadings 1–3 H_2O/BAS with Brønsted–type (B) and Lewis–type (L) approach to the active site.

	MP2:PBE+D2	revPBE+D3	revPBE+D2	PBE+D2
B	0.10	0.12	0.14	0.19
L	–	–	–	–
BH – ion-pair complex	0.91	0.91	0.93	0.92
BH – neutral complex	0.14	0.21	0.22	0.30
BL	0.05	0.07	0.07	0.11
BHH	0.91	0.91	0.92	0.92
BHL	0.12	0.18	0.18	0.25
MAD	reference	0.03	0.04	0.08

S2 Structures and Energies

S2.1   Cell Vector Optimisation

Table S18 presents the optimised cell vectors for each active site location. The cell vector lengths vary significantly between active site locations, indicating the need for separate optimisation.

Table S18: Edge lengths (*a, b, c)* in Å and cell volumes (*V*) in Å^3 for H–MFI unit cells (289 atoms with Si/Al = 95) with different active site locations as obtained by PBE+D2 cell vector optimisation (energy cutoff: 800 eV).

	a	*b*	*c*	*V*
Al2–O7(H)–Si6	20.183	19.919	13.419	5394.776
Al3–O5(H)–Si2	20.267	19.769	13.418	5376.033
Al6–O10(H)–Si3	20.163	19.886	13.435	5386.917
Al7–O17(H)–Si8	20.224	19.980	13.478	5446.130
Al11–O24(H)–Si10	20.331	19.731	13.379	5366.999
Al12–O8(H)–Si3	20.224	19.980	13.478	5446.130

S2.2   Sampling of Adsorption Structures with PBE+D2

Tables S19–S24 present the results obtained at the PBE+D2 level, comprising the number of conformers found for each interaction motif at each framework position as well as adsorption energies averaged over all conformers and for the respective most stable conformer. Further, standard deviations of adsorption energies and structural descriptors are given. Figure S5 presents the distributions of adsorption energies for each interaction motif. Figure S6 presents the respective adsorption energy differences referenced to the most stable conformer at the respective framework position. Both figures are based on the results for all six framework positions. Figure S7 shows the adsorption energy ranges divided by the number of water molecules.

Table S19: For Al2–O7(H)–Si6, PBE+D2 adsorption energies in kJ mol^{-1} for the respective most stable conformer (E_{max}) and averaged over all conformers (E_{avg}) as well as degrees of deprotonation (*DoD*) and Al–OH$_2$ bond lengths (R_{Al-OH2}) in pm for the respective most stable conformer. Standard deviations of adsorption energies (σ) in kJ mol^{-1} and number of conformers (*N*).

	1 H$_2$O/BAS		2 H$_2$O/BAS			3 H$_2$O/BAS			
	B	L	BH	BL	LH	BHH	LHH	BHL	BLH
E_{max}	−69.7	−69.8	−162.2	−128.5	−147.0	−245.1	−206.5	−204.7	−205.0
E_{avg}	−66.5	−67.2	−144.4	−121.2	−137.2	−235.4	−195.9	−193.3	−194.4
σ	2.4	3.0	15.2	5.8	6.7	7.4	7.7	7.0	6.1
N	7	4	9	16	10	17	19	15	21
DoD	0.07	–	0.95	0.04	–	0.94	–	0.18	0.02
R_{Al-OH2}	–	208.6	–	215.8	196.0	–	194.6	219.2	198.9

Table S20: For Al3–O5(H)–Si2, PBE+D2 adsorption energies in kJ mol^{-1} for the respective most stable conformer (E_{max}) and averaged over all conformers (E_{avg}) as well as degrees of deprotonation (DoD) and Al–OH$_2$ bond lengths (R_{Al-OH2}) in pm for the respective most stable conformer. Standard deviations of adsorption energies (σ) in kJ mol^{-1} and number of conformers (N).

	1 H$_2$O/BAS			2 H$_2$O/BAS			3 H$_2$O/BAS
	B	L	L^{syn}	BH	BL	BL^{syn}	BHH
E_{max}	−90.0	50.1	−29.3	−176.6	−28.4	−135.8	−246.3
E_{avg}	−86.1	53.4	−21.4	−165.4	−27.9	−114.8	−235.5
σ	3.2	2.4	10.6	6.1	0.6	18.6	9.3
N	12	4	3	13	2	4	17
DoD	0.17	–	–	0.94	0.15	0.21	0.95
R_{Al-OH2}	–	198	229	–	201	223	–

Table S21: For Al6–O10(H)–Si3, PBE+D2 adsorption energies in kJ mol^{-1} for the respective most stable conformer (E_{max}) and averaged over all conformers (E_{avg}) as well as degrees of deprotonation (DoD) and Al–OH$_2$ bond lengths (R_{Al-OH2}) in pm for the respective most stable conformer. Standard deviations of adsorption energies (σ) in kJ mol^{-1} and number of conformers (N).

	1 H$_2$O/BAS		2 H$_2$O/BAS			3 H$_2$O/BAS			
	B	L	BH	BL	LH	BHH	LHH	BHL	BLH
E_{max}	−71.8	−69.2	−162.6	−128.5	−145.9	−239.5	−205.0	−195.7	−199.6
E_{avg}	−65.3	−68.3	−149.1	−120.1	−139.7	−227.1	−197.7	−185.5	−193.2
σ	4.5	1.5	8.0	4.7	5.3	8.0	4.9	6.4	4.0
N	6	3	9	15	9	23	18	16	19
DoD	0.06	–	0.37	0.02	–	0.93	–	0.18	0.01
R_{Al-OH2}	–	205.7	–	207.1	195.1	–	190.1	216.8	197.5

Table S22: For Al7–O17(H)–Si8, PBE+D2 adsorption energies in kJ mol^{-1} for the respective most stable conformer (E_{max}) and averaged over all conformers (E_{avg}) as well as degrees of deprotonation (DoD) and Al–OH$_2$ bond lengths (R_{Al-OH2}) in pm for the respective most stable conformer. Standard deviations of adsorption energies (σ) in kJ mol^{-1} and number of conformers (N).

	1 H$_2$O/BAS		2 H$_2$O/BAS			3 H$_2$O/BAS			
	B	L	BH	BL	LH	BHH	LHH	BHL	BLH
E_{max}	−88.5	−69.2	−172.3	−144.5	−131.8	−250.4	−200.3	−210.1	−197.8
E_{avg}	−81.7	−61.1	−164.2	−139.2	−129.2	−235.5	−188.7	−202.9	−185.8
σ	5.9	7.1	7.3	3.3	1.6	9.0	8.3	7.3	6.4
N	7	5	11	19	6	15	8	12	12
DoD	0.16	–	0.89	0.05	–	0.93	–	0.16	0.03
R_{Al-OH2}	–	203	–	207	195	–	192	210	202

Table S23: For Al11–O24(H)–Si10, PBE+D2 adsorption energies in kJ mol^{-1} for the respective most stable conformer (E_{max}) and averaged over all conformers (E_{avg}) as well as degrees of deprotonation (*DoD*) and Al–OH$_2$ bond lengths (R_{Al-OH2}) in pm for the respective most stable conformer. Standard deviations of adsorption energies (σ) in kJ mol^{-1} and number of conformers (*N*).

	1 H$_2$O/BAS		2 H$_2$O/BAS				3 H$_2$O/BAS			
	B	L	BH	BL	LH	BL^{syn}	BHH	LHH	BHL	BLH
E_{max}	−96.8	−72.9	−161.7	−149.3	−133.7	−93.9	−233.7	−201.5	−203.8	−210.5
E_{avg}	−93.2	−61.4	−147.3	−136.7	−127.8	−85.1	−219.3	−191.5	−187.2	−199.3
σ	5.1	7.0	11.3	6.8	4.6	10.3	12.1	7.3	7.3	6.6
N	2	8	11	8	9	3	13	12	10	17
DoD	0.15	–	0.82	0.04	–	0.05	0.95	–	0.20	0.03
R_{Al-OH2}	–	206	–	214	195	206	–	185	204	197

Table S24: For Al12–O8(H)–Si3, PBE+D2 adsorption energies in kJ mol^{-1} for the respective most stable conformer (E_{max}) and averaged over all conformers (E_{avg}) as well as degrees of deprotonation (*DoD*) and Al–OH$_2$ bond lengths (R_{Al-OH2}) in pm for the respective most stable conformer. Standard deviations of adsorption energies (σ) in kJ mol^{-1} and number of conformers (*N*).

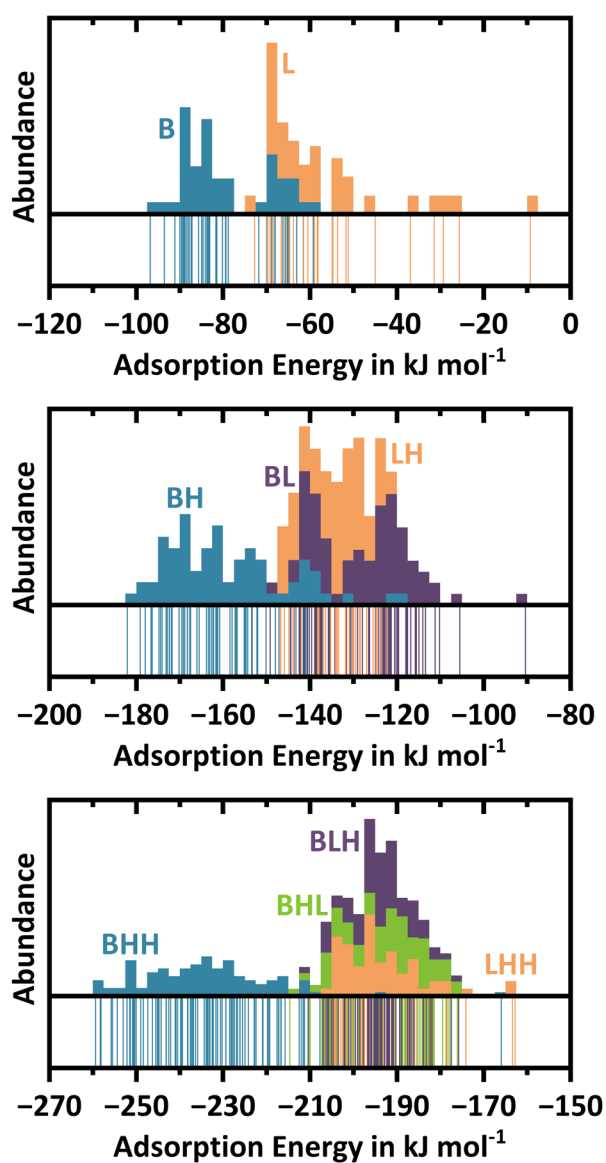|	1 H$_2$O/BAS			2 H$_2$O/BAS				3 H$_2$O/BAS	
	B	L	L^{syn}	BH	BL	LH	BL^{syn}	BHH	BHL
E_{max}	−93.5	−54.8	−30.9	−182.2	−130.0	−13.0	−126.7	−259.3	−214.7
E_{avg}	−86.0	−44.3	−3.6	−173.0	−121.8	−13.0	−82.4	−247.7	−197.8
σ	4.9	10.2	38.6	6.4	6.2	–	36.6	19.1	9.1
N	10	5	2	16	9	1	5	22	6
DoD	0.19	–	–	0.92	0.11	–	0.19	0.92	0.25
R_{Al-OH2}	–	206	207	–	213	201	210	–	221

Figure S5: Stacked histograms (bin size 2.5 kJ mol^{-1}) for loadings of 1 (top), 2 (middle) and 3 (bottom) H$_2$O/BAS, visualising the distribution of PBE+D2 adsorption energies among the conformers for each interaction motif in kJ mol^{-1}. Abundance normalised for each interaction motif. Colour code: B/BH/BHH – blue, L/LH/LHH – orange, BL/BLH – purple, BHL – green.

Figure S6: Stacked histograms (bin size 1 kJ mol⁻¹) of adsorption energy differences (ΔE) referenced to the most stable conformer at the respective framework position. Based on the PBE+D2 results for all framework positions. Abundance normalised for each interaction motif. Colour code: B/BH/BHH – blue, L/LH/LHH – orange, BL/BLH – purple, BHL – green.

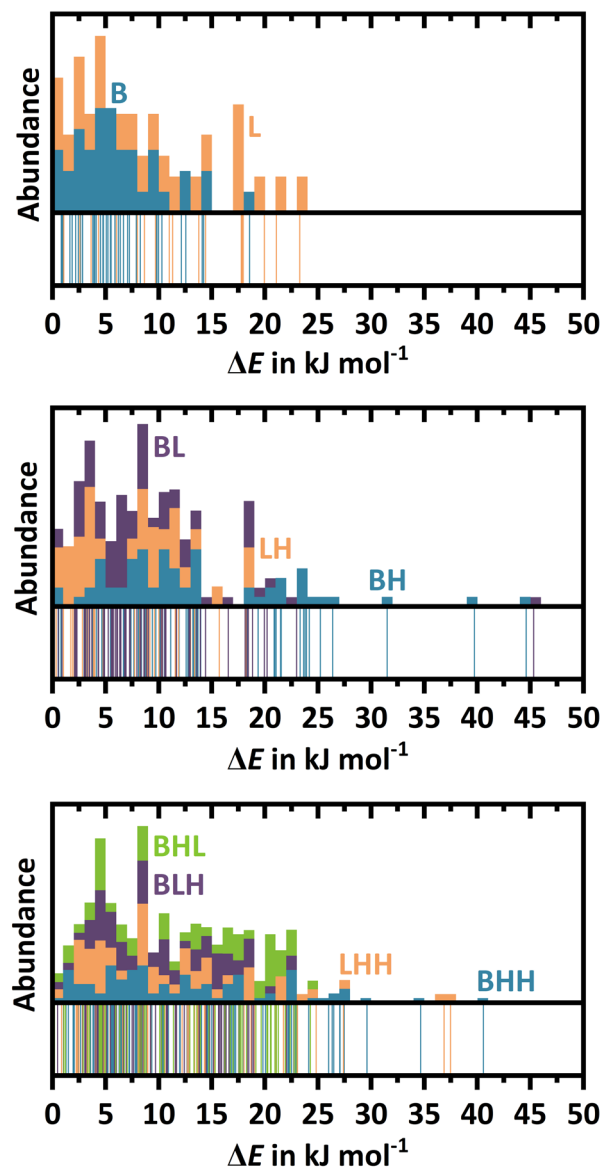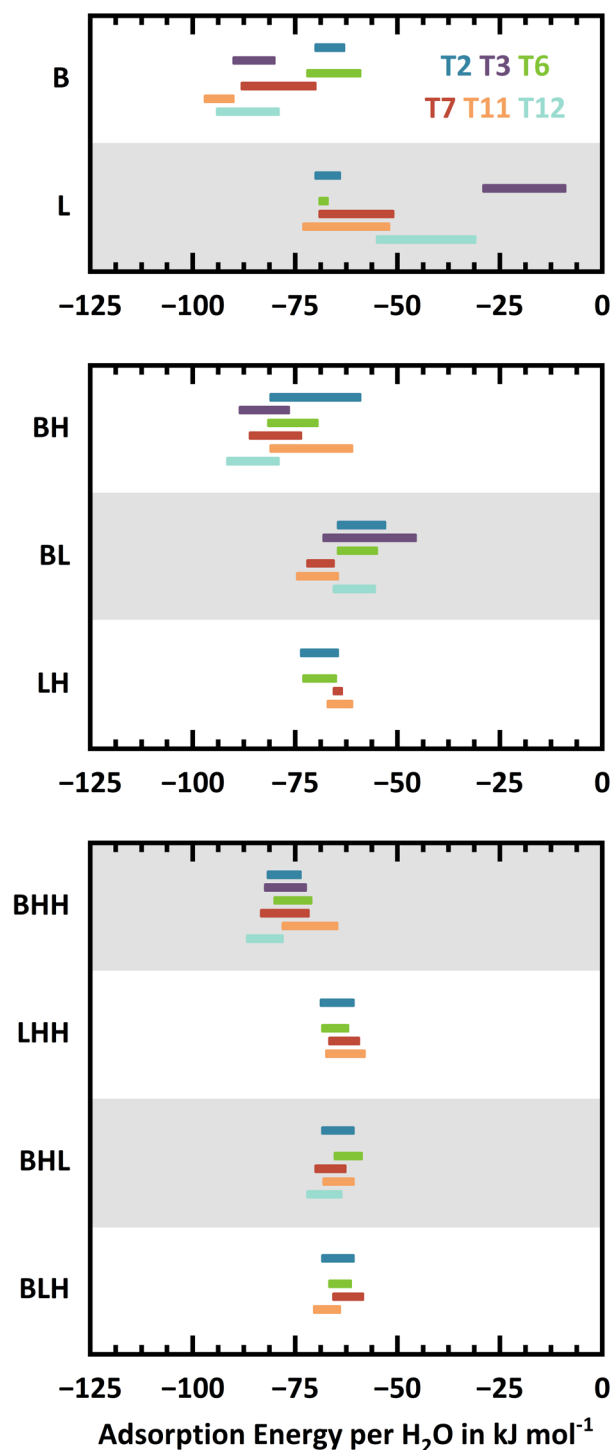**Figure S7:** Adsorption energy ranges per water molecule for conformers of water adsorption structures as obtained with PBE+D2. Colour code (top to bottom for each interaction motif): Al2–O7(H)–Si6 (T2) - blue, Al3–O5(H)–Si2 (T3) - violet, Al6–O10(H)–Si3 (T6) - green, Al7–O17(H)–Si8 (T7) - red, Al11–O24(H)–Si10 (T11) - orange, and Al12–O8(H)–Si3 (T12) - turquoise.

S2.3   Reoptimisation of PBE+D2 Structures with MP2:PBE+D2

Tables S25–S31 show the results of reoptimisation of PBE+D2 structures with B3LYP+D3:PBE+D2 or MP2:PBE+D2. As for that, adsorption energies and structural descriptors are given.

Table S25: For Al2–O7(H)–Si6, PBE+D2 (PBE), B3LYP+D3:PBE+D2 (B3LYP), and MP2:PBE+D2 (MP2) total adsorption energies (E_{ads}) in kJ mol^{-1}. Structures optimised at the respective levels of theory. Degrees of deprotonation (DoD), Al–OH$_2$ bond lengths ($R_{Al–OH2}$) in pm, and mean absolute deviations (MAD) in pm of all OH bond lengths relative to the MP2:PBE+D2 structures.

		1 H$_2$O/BAS		2 H$_2$O/BAS			3 H$_2$O/BAS			
		B	L	BH	BL	LH	BHH	LHH	BHL	BLH
PBE	E_{ads}	−69.7	−69.9	−162.2	−128.5	−147.0	−245.1	−206.5	−204.7	−205.0
	DoD	0.07	–	0.94	0.04	–	0.94	–	0.18	0.02
	$R_{Al\text{-}OH2}$	–	208.8	–	215.8	196.0	–	194.6	219.2	198.9
	MAD	5.0	2.6	8.9	3.8	2.7	4.1	9.3	7.5	3.8
B3LYP	E_{ads}	−65.7	−62.9	−138.5	−114.6	−135.1	−219.8	−188.2	−182.5	−186.8
	DoD	0.04	–	0.93	0.02	–	0.95	–	0.08	0.01
	$R_{Al\text{-}OH2}$	–	207.2	–	215.6	195.4	–	194.1	216.3	198.2
	MAD	0.4	0.9	1.0	1.6	0.2	3.5	0.2	1.0	0.4
MP2	E_{ads}	−61.0	−66.1	−127.2	−112.9	−135.0	−205.7	−185.7	−175.2	−182.7
	DoD	0.04	–	0.92	0.02	–	0.95	–	0.07	0.01
	$R_{Al\text{-}OH2}$	–	205.4	–	212.3	195.3	–	194.3	212.7	198.0
	MAD	0.0	0.0	0.0	0.0	0.0	0.0	0.0	0.0	0.0

Table S26: For Al3–O5(H)–Si2, PBE+D2 (PBE), B3LYP+D3:PBE+D2 (B3LYP), and MP2:PBE+D2 (MP2) total adsorption energies (E_{ads}) in kJ mol^{-1}. Structures optimised at the respective levels of theory. Degrees of deprotonation (*DoD*), Al–OH$_2$ bond lengths (R_{Al-OH2}) in pm, and mean absolute deviations (MAD) in pm of all OH bond lengths relative to the MP2:PBE+D2 structures.

		1 H$_2$O/BAS		2 H$_2$O/BAS			3 H$_2$O/BAS			
		B	L^{syn}	BH	BL^{syn}	LH	BHH	LHH	BHL	BLH
PBE	E_{ads}	−90.0	−29.3	−176.6	−138.7	–	−246.3	–	–	–
	DoD	0.18	–	0.93	0.21	–	0.96	–	–	–
	R_{Al-OH2}	–	229.4	–	219.2	–	–	–	–	–
	MAD	8.1	4.9	4.2	5.6	–	2.5	–	–	–
B3LYP	E_{ads}	−78.5	−20.5	−152.4	−113.5	–	−213.8	–	–	–
	DoD	0.09	–	0.94	0.11	–	0.97	–	–	–
	R_{Al-OH2}	–	227.6	–	224.9	–	–	–	–	–
	MAD	0.3	3.2	2.0	2.4	–	0.4	–	–	–
MP2	E_{ads}	−71.4	−19.4	−147.3	−105.7	–	−196.0	–	–	–
	DoD	0.08	–	0.92	0.10	–	0.97	–	–	–
	$R_{Al–OH2}$	–	221.3	–	218.3	–	–	–	–	–
	MAD	0.0	0.0	0.0	0.0	–	0.0	–	–	–

Table S27: For Al6–O10(H)–Si3, PBE+D2 (PBE), B3LYP+D3:PBE+D2 (B3LYP), and MP2:PBE+D2 (MP2) total adsorption energies (E_{ads}) in kJ mol^{-1}. Structures optimised at the respective levels of theory. Degrees of deprotonation (*DoD*), Al–OH$_2$ bond lengths (R_{Al-OH2}) in pm, and mean absolute deviations (MAD) in pm of all OH bond lengths relative to the MP2:PBE+D2 structures.

		1 H$_2$O/BAS		2 H$_2$O/BAS			3 H$_2$O/BAS			
		B	L	BH	BL	LH	BHH	LHH	BHL	BLH
PBE	E_{ads}	−71.8	−69.2	−162.6	−128.5	−145.9	−239.6	−205.1	−195.7	−199.6
	DoD	0.06	–	0.92	0.03	–	0.93	–	0.18	0.01
	$R_{Al–OH2}$	–	205.8	–	207.1	195.1	–	190.2	216.8	197.3
	MAD	5.5	2.3	5.8	3.3	2.7	3.6	3.7	7.7	3.2
B3LYP	E_{ads}	−66.7	−62.5	−139.4	−116.9	−135.4	−212.9	−186.7	−173.8	−180.1
	DoD	0.03	–	0.91	0.02	–	0.93	–	0.07	0.00
	$R_{Al–OH2}$	–	204.2	–	206.7	193.8	–	189.3	214.2	196.3
	MAD	0.5	0.6	0.8	0.8	0.7	0.8	0.9	0.9	0.9
MP2	E_{ads}	−61.3	−65.2	−128.7	−114.7	−135.0	−197.3	−182.6	−165.1	−175.7
	DoD	0.03	–	0.91	0.02	–	0.92	–	0.07	0.01
	$R_{Al–OH2}$	–	203.0	–	205.2	194.6	–	190.9	211.1	197.1
	MAD	0.0	0.0	0.0	0.0	0.0	0.0	0.0	0.0	0.0

Table S28: For Al7–O17(H)–Si8, PBE+D2 (PBE), B3LYP+D3:PBE+D2 (B3LYP), and MP2:PBE+D2 (MP2) total adsorption energies (E_{ads}) in kJ mol^{-1}. Structures optimised at the respective levels of theory. Degrees of deprotonation (*DoD*), Al–OH$_2$ bond lengths (R_{Al-OH2}) in pm, and mean absolute deviations (MAD) in pm of all OH bond lengths relative to the MP2:PBE+D2 structures.

		1 H$_2$O/BAS		2 H$_2$O/BAS			3 H$_2$O/BAS			
		B	L	BH	BL	LH	BHH	LHH	BHL	BLH
PBE	E_{ads}	−88.5	−69.2	−172.3	−144.5	−131.8	−250.4	−201.5	−210.1	−197.8
	DoD	0.15	–	0.89	0.06	–	0.92	–	0.17	0.04
	R_{Al-OH2}	–	202.7	–	207.4	194.8	–	191.6	210.0	202.3
	MAD	8.3	1.3	5.1	4.1	2.6	2.9	3.8	6.7	3.4
B3LYP	E_{ads}	−83.2	−62.4	−150.9	−128.1	−118.0	−222.5	−180.6	−187.9	−176.6
	DoD	0.07	–	0.89	0.03	–	0.93	–	0.07	0.02
	R_{Al-OH2}	–	202.2	–	206.3	194.8	–	192.3	208.8	201.9
	MAD	0.3	0.5	0.7	1.2	0.3	0.4	0.3	0.9	0.7
MP2	E_{ads}	−73.7	−62.9	−136.7	−124.8	−113.8	−201.5	−174.2	−175.6	−170.4
	DoD	0.06	–	0.88	0.03	–	0.92	–	0.06	0.02
	R_{Al-OH2}	–	201.1	–	203.9	194.6	–	192.6	206.3	200.6
	MAD	0.0	0.0	0.0	0.0	0.0	0.0	0.0	0.0	0.0

Table S29: For Al11–O24(H)–Si10, PBE+D2 (PBE), B3LYP+D3:PBE+D2 (B3LYP), and MP2:PBE+D2 (MP2) total adsorption energies (E_{ads}) in kJ mol^{-1}. Structures optimised at the respective levels of theory. Degrees of deprotonation (*DoD*), Al–OH$_2$ bond lengths (R_{Al-OH2}) in pm, and mean absolute deviations (MAD) in pm of all OH bond lengths relative to the MP2:PBE+D2 structures.

		1 H$_2$O/BAS		2 H$_2$O/BAS			3 H$_2$O/BAS			
		B	L	BH	BL	LH	BHH	LHH	BHL	BLH
PBE	E_{ads}	−96.8	−72.9	−161.7	−149.3	−133.7	−233.7	−201.5	−203.8	−210.5
	DoD	0.15	–	0.82	0.04	–	0.96	–	0.20	0.02
	R_{Al-OH2}	–	206.3	–	214.1	195.3	–	185.2	215.5	197.4
	MAD	6.5	1.4	3.2	5.1	3.0	2.5	4.8	6.6	3.1
B3LYP	E_{ads}	−87.4	−63.4	−140.9	−134.2	−116.3	−206.6	−180.1	−180.9	−190.1
	DoD	0.07	–	0.85	0.01	–	0.98	–	0.08	0.00
	R_{Al-OH2}	–	205.6	–	217.7	195.4	–	185.3	213.2	197.1
	MAD	0.4	0.6	1.7	3.0	0.4	0.9	0.6	0.7	0.6
MP2	E_{ads}	−77.8	−65.4	−128.2	−128.5	−111.5	−191.5	−168.6	−171.8	−180.4
	DoD	0.07	–	0.82	0.01	–	0.97	–	0.07	0.00
	R_{Al-OH2}	–	204.5	–	209.4	195.6	–	185.7	211.0	196.0
	MAD	0.0	0.0	0.0	0.0	0.0	0.0	0.0	0.0	0.0

Table S30: For Al12–O8(H)–Si3, PBE+D2 (PBE), B3LYP+D3:PBE+D2 (B3LYP), and MP2:PBE+D2 (MP2) total adsorption energies (E_{ads}) in kJ mol^{-1}. Structures optimised at the respective levels of theory. Degrees of deprotonation (*DoD*), Al–OH$_2$ bond lengths (R_{Al-OH2}) in pm, and mean absolute deviations (MAD) in pm of all OH bond lengths relative to the MP2:PBE+D2 structures.

		1 H$_2$O/BAS		2 H$_2$O/BAS			3 H$_2$O/BAS			
		B	L	BH	BL	LH	BHH	LHH	BHL	BLH
PBE	E_{ads}	−93.5	−54.8	−182.2	−130.0	–	−259.3	–	−214.7	–
	DoD	0.19	–	0.93	0.11	–	0.92	–	0.25	–
	R_{Al-OH2}	–	206.2	–	213.0	–	–	–	221.1	–
	MAD	6.9	1.4	4.8	4.8	–	4.4	–	9.2	–
B3LYP	E_{ads}	−82.4	−44.9	−153.2	−111.9	–	−229.3	–	−185.6	–
	DoD	0.10	–	0.93	0.06	–	0.92	–	0.12	–
	R_{Al-OH2}	–	206.1	–	215.1	–	–	–	222.1	–
	MAD	0.8	0.9	1.7	1.2	–	2.6	–	1.6	–
MP2	E_{ads}	−78.0	−47.1	−141.4	−110.1	–	−217.8	–	−175.7	–
	DoD	0.10	–	0.91	0.05	–	0.91	–	0.12	–
	R_{Al-OH2}	–	204.4	–	211.7	–	–	–	216.6	–
	MAD	0.0	0.0	0.0	0.0	–	0.0	–	0.0	–

Table S31: Overview over degrees of deprotonation as obtained with PBE+D2 (PBE) and MP2:PBE+D2 (MP2) at all framework positions (indicated by Al position). Structures optimised at the respective levels of theory.

		1 H$_2$O/BAS		2 H$_2$O/BAS			3 H$_2$O/BAS			
		B	L	BH	BL	LH	BHH	LHH	BHL	BLH
T2	PBE	0.07	–	0.94	0.04	–	0.94	–	0.18	0.02
	MP2	0.04	–	0.92	0.02	–	0.95	–	0.07	0.01
T3	PBE	0.18	–	0.93	0.21	–	0.96	–	–	–
	MP2	0.08	–	0.92	0.10	–	0.97	–	–	–
T6	PBE	0.06	–	0.92	0.03	–	0.93	–	0.18	0.01
	MP2	0.03	–	0.91	0.02	–	0.92	–	0.07	0.01
T7	PBE	0.15	–	0.89	0.06	–	0.92	–	0.17	0.04
	MP2	0.06	–	0.88	0.03	–	0.92	–	0.06	0.02
T11	PBE	0.15	–	0.82	0.04	–	0.96	–	0.20	0.02
	MP2	0.07	–	0.82	0.01	–	0.97	–	0.07	0.00
T12	PBE	0.19	–	0.93	0.11	–	0.92	–	0.25	–
	MP2	0.10	–	0.91	0.05	–	0.91	–	0.12	–

S2.4 MP2:(PBE+D2)+ΔCC Adsorption Enthalpies

Tables S32–S33 present MP2:(PBE+D2)+ΔCC electronic energies as well as PBE+D2 zero–point vibrational energy corrections and thermal enthalpy contributions used to obtain the benchmark water adsorption enthalpies at 298 K that are presented in Table 2 in the main text. Tables S34–S35 present the MP2 and CCSD(T) corrections contributing to the hybrid MP2:(PBE+D2)+ΔCC electronic energies.

Table S32: For 1 H_2O/BAS and 2 H_2O/BAS, MP2:(PBE+D2)+ΔCC adsorption energies (E_{ads}) as well as PBE+D2 zero–point energy contributions (ΔZPVE) and thermal enthalpy contributions at 298 K ($\Delta H_{0\,K\rightarrow298\,K}$) used to calculate benchmark adsorption enthalpies at 298 K (H_{ads}) in kJ mol^{-1}. MP2:(PBE+D2)+ΔCC single–point energy calculations with cc–pVnZ (n = T,Q) basis set extrapolation and Counterpoise correction for cluster calculations. PBE+D2 within the harmonic approximation to obtain zero–point energy contributions and thermal enthalpy contributions.

		1 H_2O/BAS		2 H_2O/BAS		
		B	L	BH	BL	LH
T2	E_{ads}	−63.7	−67.0	−123.2	−115.6	−132.8
	ΔZPVE	9.2	11.2	15.9	19.3	21.0
	$\Delta H_{0K\rightarrow298K}$	−2.7	−3.8	−8.7	−5.8	−7.6
	H_{ads}	−57.1	−59.6	−116.0	−102.1	−119.5
T3	E_{ads}	−74.2	−25.0[a]	−139.3	−110.5[b]	–
	ΔZPVE	9.6	10.8[a]	20.7	19.7[b]	–
	$\Delta H_{0K\rightarrow298K}$	−5.1	−4.0[a]	−10.1	−9.8[b]	–
	H_{ads}	−69.8	−18.2[a]	−128.6	−100.6[b]	–
T6	E_{ads}	−67.0	−64.4	−124.4	−122.7	−132.7
	ΔZPVE	8.0	11.0	16.1	19.1	19.6
	$\Delta H_{0K\rightarrow298K}$	−1.6	−3.4	−8.1	−5.4	−6.5
	H_{ads}	−60.6	−56.8	−116.4	−109.1	−119.6
T7	E_{ads}	−74.3	−62.8	−128.4	−128.0	−119.1
	ΔZPVE	3.9	7.6	12.2	18.6	17.5
	$\Delta H_{0K\rightarrow298K}$	−2.2	−2.6	−8.3	−6.4	−6.0
	H_{ads}	−72.6	−57.8	−124.5	−115.8	−107.6
T11	E_{ads}	−72.5	−63.2	−111.6	−125.4	−112.5
	ΔZPVE	9.6	13.1	15.1	22.4	16.9
	$\Delta H_{0K\rightarrow298K}$	−5.9	−4.8	−8.7	−8.9	−5.4
	H_{ads}	−68.7	−54.9	−105.3	−111.9	−101.0
T12	E_{ads}	−78.9	−44.7	−136.3	−108.5	–
	ΔZPVE	7.6	13.1	20.6	21.8	–
	$\Delta H_{0K\rightarrow298K}$	−4.6	−5.4	−10.8	−8.9	–
	H_{ads}	−75.9	−37.0	−126.5	−95.6	–

[a] L^{syn} [b] BL^{syn}

Table S33: For 3 H$_2$O/BAS, MP2:(PBE+D2)+ΔCC adsorption energies (E_{ads}) as well as PBE+D2 zero–point energy contributions (ΔZPVE) and thermal enthalpy contributions at 298 K ($\Delta H_{0\,K\rightarrow298\,K}$) used to calculate benchmark adsorption enthalpies at 298 K (H_{ads}) in kJ mol^{-1}. MP2:(PBE+D2)+ΔCC single–point energy calculations with cc–pVnZ (n = T,Q) basis set extrapolation and Counterpoise correction for cluster calculations. PBE+D2 within the harmonic approximation to obtain zero–point energy contributions and thermal enthalpy contributions.

		3 H$_2$O/BAS			
		BHH	LHH	BHL	BLH
T2	E_{ads}	−197.8	−181.1	−178.0	−183.2
	ΔZPVE	29.5	30.0	27.5	29.6
	$\Delta H_{0K\rightarrow298K}$	−12.3	−10.4	−10.5	−9.9
	H_{ads}	−180.6	−161.5	−161.0	−163.5
T3	E_{ads}	−191.0	–	–	–
	ΔZPVE	25.6	–	–	–
	$\Delta H_{0K\rightarrow298K}$	−12.5	–	–	–
	H_{ads}	−177.9	–	–	–
T6	E_{ads}	−196.8	−176.2	−167.2	−179.0
	ΔZPVE	30.6	30.3	26.2	29.3
	$\Delta H_{0K\rightarrow298K}$	−12.1	−10.2	−9.9	−8.5
	H_{ads}	−178.3	−156.2	−150.9	−158.1
T7	E_{ads}	−200.6	−174.3	−177.2	−174.2
	ΔZPVE	27.2	27.5	24.0	26.6
	$\Delta H_{0K\rightarrow298K}$	−12.6	−9.9	−10.2	−8.2
	H_{ads}	−185.9	−156.8	−163.4	−155.8
T11	E_{ads}	−180.6	−165.8	−165.6	−176.4
	ΔZPVE	26.2	24.4	25.9	33.7
	$\Delta H_{0K\rightarrow298K}$	−13.4	−9.2	−11.1	−12.7
	H_{ads}	−167.8	−150.5	−150.8	−155.4
T12	E_{ads}	−207.0	–	−176.6	–
	ΔZPVE	29.2	–	30.1	–
	$\Delta H_{0K\rightarrow298K}$	−13.1	–	−13.4	–
	H_{ads}	−190.9	–	−159.9	–

Table S34: For 1 H_2O/BAS and 2 H_2O/BAS, MP2 (ΔMP2) and CCSD(T) (ΔCC) corrections contributing to the MP2:(PBE+D2)+ΔCC adsorption energies in kJ mol^{-1}. MP2:(PBE+D2)+ΔCC single–point energy calculations with cc–pVnZ (n = T,Q) basis set extrapolation and Counterpoise correction for cluster calculations.

		1 H_2O/BAS		2 H_2O/BAS		
		B	L[a]	BH	BL[a]	LH
T2	ΔMP2	5.1	3.5	34.2	13.9	13.6
	ΔCC	−1.0	−1.3	3.1	−2.9	−1.0
T3	ΔMP2	13.5	4.8	33.0	22.1	–
	ΔCC	−0.4	−1.3	3.2	0.4	–
T6	ΔMP2	2.1	5.1	34.4	5.6	12.5
	ΔCC	−1.0	−0.8	2.1	−1.9	−0.6
T7	ΔMP2	10.2	6.0	36.0	14.7	10.2
	ΔCC	1.8	−0.2	6.2	−0.2	0.0
T11	ΔMP2	21.3	9.0	42.5	22.3	18.1
	ΔCC	1.1	−0.4	5.9	−1.1	−0.7
T12	ΔMP2	11.4	10.4	39.2	19.5	–
	ΔCC	0.9	−0.9	4.6	−0.5	–

[a] L^{syn} and BL^{syn} for T3

Table S35: For 3 H_2O/BAS, MP2 (ΔMP2) and CCSD(T) (ΔCC) corrections contributing to the MP2:(PBE+D2)+ΔCC adsorption energies in kJ mol^{-1}. MP2:(PBE+D2)+ΔCC single–point energy calculations with cc–pVnZ (n = T,Q) basis set extrapolation and Counterpoise correction for cluster calculations.

		3 H_2O/BAS			
		BHH	LHH	BHL	BLH
T2	ΔMP2	40.9	23.8	24.5	19.4
	ΔCC	2.4	−0.8	−1.2	−1.9
T3	ΔMP2	49.7	–	–	–
	ΔCC	3.8	–	–	–
T6	ΔMP2	37.4	26.5	25.3	20.0
	ΔCC	2.2	−0.1	−1.0	−2.4
T7	ΔMP2	41.6	24.7	27.3	20.3
	ΔCC	5.7	0.0	1.3	−0.3
T11	ΔMP2	45.0	31.4	33.7	32.4
	ΔCC	6.0	1.0	1.2	−0.9
T12	ΔMP2	44.3	–	32.9	–
	ΔCC	4.6	–	1.3	–

S3 Cluster Models

Figures S7–S18 illustrate the cluster models used in hybrid MP2:PBE+D2 structure optimisations and MP2:(PBE+D2)+ΔCC single–point energy calculations.
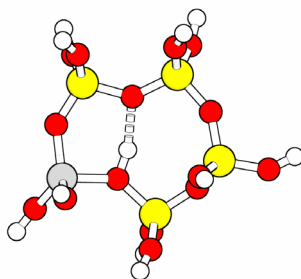

Figure S8: Cluster used for MP2:PBE+D2 structure optimisations and for ΔCC corrections in MP2:(PBE+D2)+ΔCC single–point energy calculations at Al2–O7(H)–Si6.
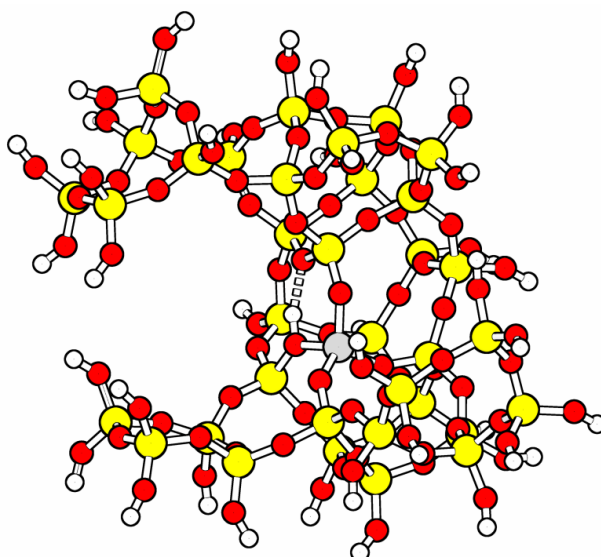

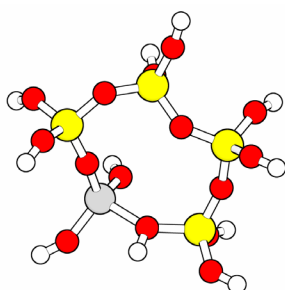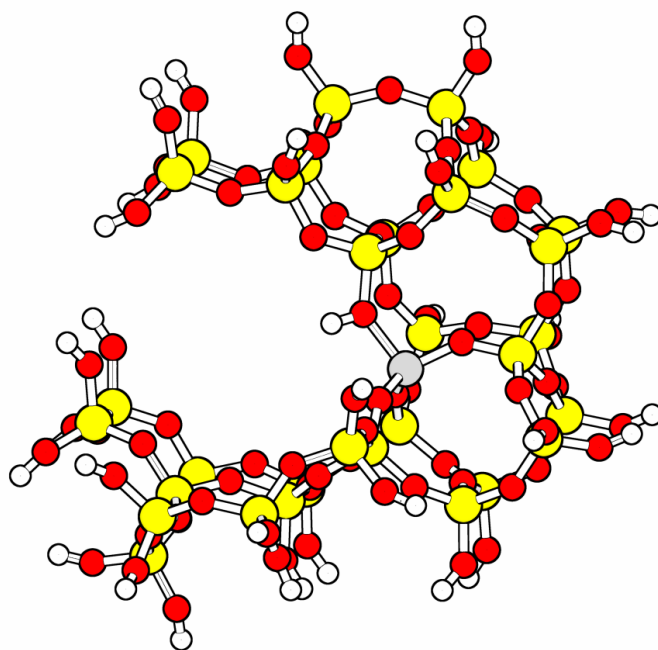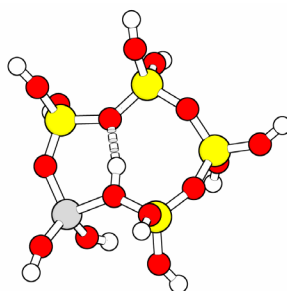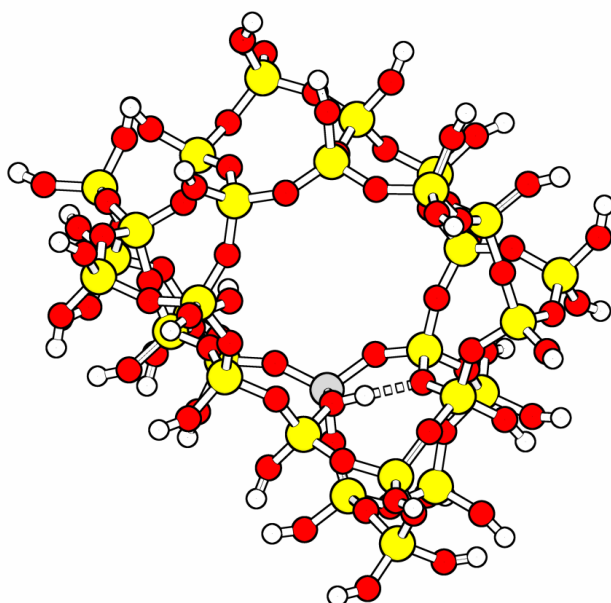**Figure S9:** Cluster used for MP2 corrections in MP2:(PBE+D2)+ΔCC single–point energy calculations at Al2–O7(H)–Si6.

Figure S10: Cluster used for MP2:PBE+D2 structure optimisations and for ΔCC corrections in MP2:(PBE+D2)+ΔCC single–point energy calculations at Al3–O5(H)–Si2.

Figure S11: Cluster used for MP2 corrections in MP2:(PBE+D2)+ΔCC single–point energy calculations at Al3–O5(H)–Si2.

Figure S12: Cluster used for MP2:PBE+D2 structure optimisations and for ΔCC corrections in MP2:(PBE+D2)+ΔCC single–point energy calculations at Al6–O10(H)–Si3.

Figure S13: Cluster used for MP2 corrections in MP2:(PBE+D2)+ΔCC single–point energy calculations at Al6–O10(H)–Si3.
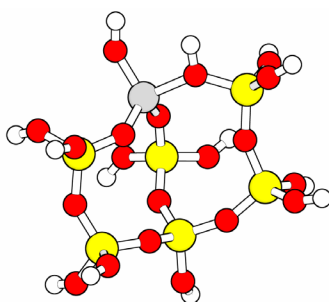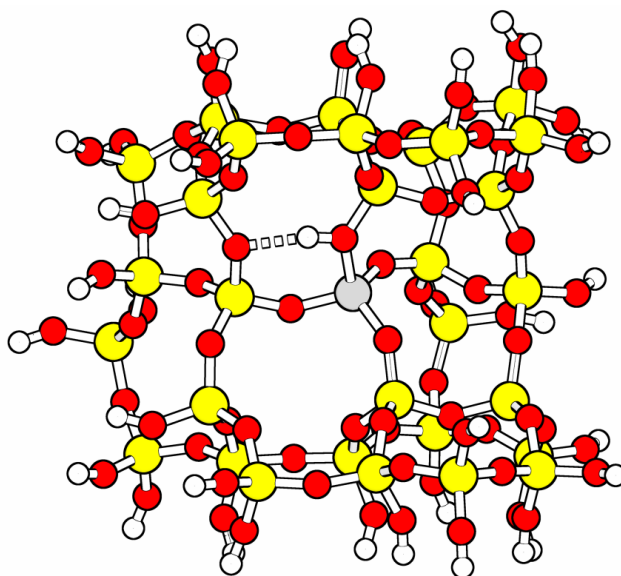

Figure S14: Cluster used for MP2:PBE+D2 structure optimisations and for ΔCC corrections in MP2:(PBE+D2)+ΔCC single–point energy calculations at Al7–O17(H)–Si8.

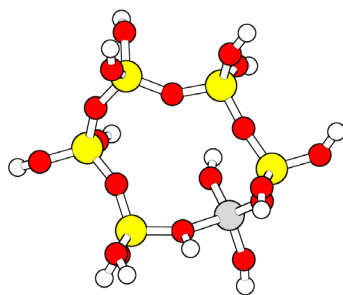**Figure S15:** Cluster used for MP2 corrections in MP2:(PBE+D2)+ΔCC single–point energy calculations at Al7–O17(H)–Si8.

Figure S16: Cluster used for MP2:PBE+D2 structure optimisations and for ΔCC corrections in MP2:(PBE+D2)+ΔCC single–point energy calculations at Al11–O24(H)–Si10.
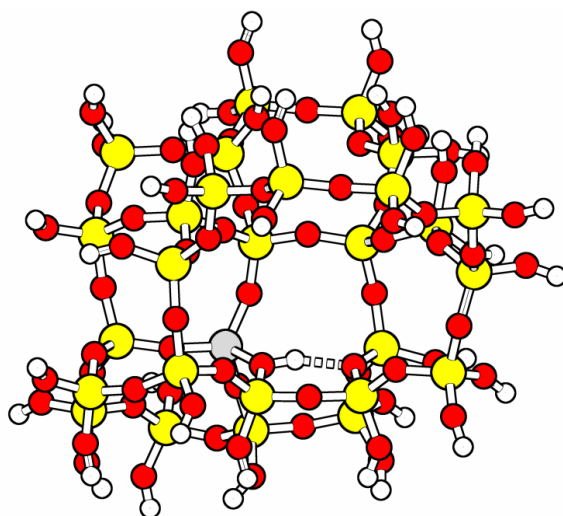

Figure S17: Cluster used for MP2 corrections in MP2:(PBE+D2)+ΔCC single–point energy calculations at Al11–O24(H)–Si10.
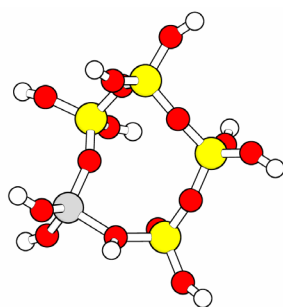

Figure S18: Cluster used for MP2:PBE+D2 structure optimisations and for ΔCC corrections in MP2:(PBE+D2)+ΔCC single–point energy calculations at Al12–O8(H)–Si3.
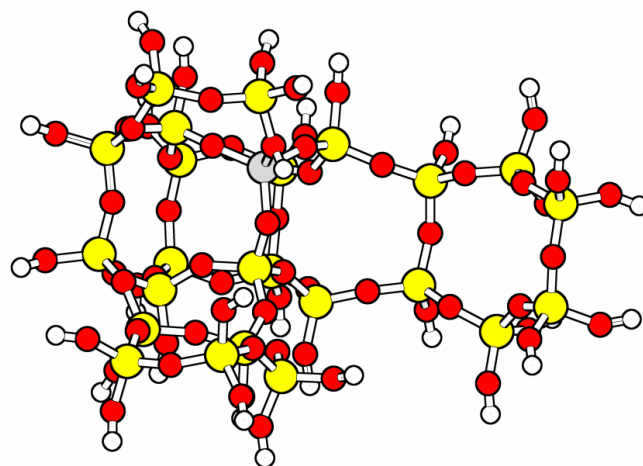
Figure S19: Cluster used for MP2 corrections in MP2:(PBE+D2)+ΔCC single–point energy calculations at Al12–O8(H)–Si3.

S4 Experimental Data

Table 36: Experimental heats of adsorption (q_{ads}) in kJ mol^{-1} from microcalorimetric measurements as reported by Lercher and co–workers[33] for an H–MFI sample with Si/Al = 45.

H$_2$O/BAS	q_{ads}		
	differential	integral	integral per molecule
0.0989	75.6756	7.48	75.68
0.2968	61.0724	21.02	70.81
0.4452	66.456	30.48	68.46
0.6925	70.0745	47.36	68.39
0.8409	81.8496	58.63	**69.73**
1.4344	78.1592	106.12	73.98
1.9785	66.9679	145.60	**73.59**
3.6602	54.0842	247.38	**67.59**
4.7978	50.0989	306.64	63.91
6.1333	45.9032	370.75	60.45
6.5784	43.8648	390.73	59.40
6.7763	43.2001	399.34	58.93
6.8257	43.0969	401.47	58.82

Table 37: Experimental heats of adsorption (q_{ads}) in kJ mol^{-1} from microcalorimetric measurements as reported by Lercher and co–workers[33] for an H–MFI sample with Si/Al = 110.

H$_2$O/BAS	q_{ads}		
	differential	integral	integral per molecule
0.1808	81.0629	14.66	81.06
0.3617	64.5624	27.83	76.94
0.633	60.5456	44.80	70.77
0.9946	80.3872	70.28	**70.66**
1.1755	85.0266	85.24	72.51
1.718	75.852	128.88	75.02
2.1701	69.8544	161.82	**74.57**
3.3456	63.2356	240.04	**71.75**
4.4307	56.0952	304.78	68.79
5.9679	49.8071	386.18	64.71
6.2391	49.012	399.58	64.04
6.6008	45.0878	416.60	63.11
6.9806	44.5364	433.62	62.12

Table 38: Averaged experimental heats of adsorption (q_{ads}) in kJ mol^{-1} quoted in the main text. The data used are printed in bold in Tables S36 and S37.

Si/Al	H_2O/BAS	q_{ads}			average	half spread
		differential	integral	integral per H_2O		
110	0.9946	80.3872	70.28	70.66	70.19	0.47
45	0.8409	81.8496	58.63	69.73		
110	2.1701	69.8544	161.82	74.57	149.78	1.43
45	1.9785	66.9679	145.60	73.59		
110	3.3456	63.2356	240.04	71.75	209.00	6.24
45	3.6602	54.0842	247.38	67.59		

S5 Homogeneous vs. Heterogeneous Distribution of H$_2$O over Adsorption Sites

In this work, we assume a homogeneous distribution of water molecules over the active sites. In this section we show that this assumption is justified. We calculate Gibbs free energies of adsorption for loadings of 1 and 2 H$_2$O/BAS, see Table S39. We consider two models for adsorption of two water molecules in two unit cells with one BAS in each of the cells:
(a) homogeneous distribution with adsorption of one H$_2$O at each BAS (2B or 2L)
(b) heterogeneous distribution with adsorption of two H$_2$O at one BAS (BH, BL, or LH) and no adsorption at the other BAS.
From Gibbs free energies of adsorption, we calculate Boltzmann-populations for both cases at 298 K (Table S39) and use these to calculate Boltzmann-weighted adsorption enthalpies, see Table S40.

Table S39: Entropy terms (−TΔS) and Gibbs free energies (ΔG) of adsorption at 298 K in kJ mol^{-1} as well as Boltzmann weights for homogeneous (1:1) and heterogeneous (2:0) distribution. The 1:1 distribution considers twice the most exergonic adsorption for 1 H$_2$O/BAS (B or L) while the 2:0 distribution considers the most exergonic adsorption for 2 H$_2$O/BAS (BH, BL or LH). Methods: MP2+ΔCC for electronic energies and PBE+D2 for vibrational partition functions.

	−TΔS					ΔG					ΔG - Distribution		Weight (%)	
	B	L^a	BH	BL^a	LH	B	L^a	BH	BL^a	LH	(1:1)	(2.0)	(1:1)	(2:0)
T2	42	48	91	91	95	−15	−12	−25	−11	−24	−30 (2B)	−25 (BH)	86	14
											−30 (2B)	−24 (LH)	90	10
T3	48	43	96	103	−	−22	25	−33	2	−	−44 (2B)	−33 (BH)	99	1
T6	38	46	90	81	90	−23	−11	−26	−28	−30	−46 (2B)	−30 (LH)	100	0
T7	46	50	98	93	95	−27	−8	−26	−23	−13	−54 (2B)	−26 (BH)	100	0
T11	57	53	99	103	90	−12	−2	−6	−9	−11	−24 (2B)	−11 (LH)	99	1
T12	48	55	101	100	−	−28	18	−26	4	−	−55 (2B)	−26 (BH)	100	0

^{a} L^{syn} and BL^{syn} for T3

Table S40: Adsorption enthalpies (ΔH) at 298 K in kJ mol^{-1}. Homogeneous distribution (1:1) considers twice the most exergonic adsorption for 1 H$_2$O/BAS (2B) while heterogeneous distribution (2:0) considers once the most exergonic adsorption for 2 H$_2$O/BAS (BH or LH). Methods: MP2+ΔCC for electronic energies and PBE+D2 for vibrational partition functions.

	B	L^a	BH	BL^a	LH	Homog. (1:1)	Heterog. (2:0)	Boltzmann− weighted mix
T2	−57	−60	−116	−102	−119	−114 (2B)	−116 (BH)	−114
						−114 (2B)	−119 (LH)	−114
T3	−70	−18	−129	−101	−	−140 (2B)	−129 (BH)	−140
T6	−61	−57	−116	−109	−120	−122 (2B)	−120 (LH)	−122
T7	−73	−58	−124	−116	−108	−146 (2B)	−124 (BH)	−146
T11	−69	−55	−105	−112	−101	−138 (2B)	−101 (LH)	−138
T12	−76	−37	−127	−96	−	−152 (2B)	−127 (BH)	−152

^{a} L^{syn} and BL^{syn} for T3

Only for T2, there is a non-negligible Boltzmann weight for the 2:0 distribution, BH and LH. Applying the weights for the 1:1 (86 and 90%) and 2:0 distributions (14 and 10%) to calculate mixed adsorption enthalpies yields a negligible change of the result for the homogeneous occupation of adsorption sites (−114 kJ mol^{-1}) for both BH and LH occupations. We conclude that taking into account heterogeneous distribution of water molecules over different adsorption sites will not change the enthalpies of adsorption to a noticeable extend.

S6 References

1. J. Sauer, *Acc. Chem. Res.*, 2019, **52**, 3502-3510.
2. G. Piccini, M. Alessio and J. Sauer, *Angew. Chem. Int. Ed.*, 2016, **55**, 5235-5237.
3. G. Piccini, M. Alessio, J. Sauer, Y. Zhi, Y. Liu, R. Kolvenbach, A. Jentys and J. A. Lercher, *J. Phys. Chem. C*, 2015, **119**, 6128-6137.
4. F. Berger and J. Sauer, *Angew. Chem. Int. Ed.*, 2021, **60**, 3529-3533.
5. F. Berger, M. Rybicki and J. Sauer, *J. Catal.*, 2021, **395**, 117-128.
6. Q. Ren, M. Rybicki and J. Sauer, *J. Phys. Chem. C*, 2020, **124**, 10067-10078.
7. C. Tuma and J. Sauer, *J. Chem. Phys.*, 2015, **143**.
8. M. Rybicki and J. Sauer, *J. Am. Chem. Soc.*, 2018, **140**, 18151-18161.
9. N. Hansen, T. Kerber, J. Sauer, A. T. Bell and F. J. Keil, *J. Am. Chem. Soc.*, 2010, **132**, 11525-11538.
10. F. Weigend and R. Ahlrichs, *Phys. Chem. Chem. Phys.*, 2005, **7**, 3297-3305.
11. T. H. Dunning, Jr., *J. Chem. Phys.*, 1989, **90**, 1007-1023.
12. D. E. Woon and T. H. Dunning, Jr., *J. Chem. Phys.*, 1993, **98**, 1358-1371.
13. R. A. Kendall, T. H. Dunning, Jr. and R. J. Harrison, *J. Chem. Phys.*, 1992, **96**, 6796-6806.
14. K. A. Peterson, D. E. Woon and T. H. Dunning, Jr., *J. Chem. Phys.*, 1994, **100**, 7410-7415.
15. A. K. Wilson, T. van Mourik and T. H. Dunning, *Journal of Molecular Structure: THEOCHEM*, 1996, **388**, 339-349.
16. A. Schäfer, H. Horn and R. Ahlrichs, *J. Chem. Phys.*, 1992, **97**, 2571-2577.
17. A. Schäfer, C. Huber and R. Ahlrichs, *J. Chem. Phys.*, 1994, **100**, 5829-5835.
18. F. Weigend, *Phys. Chem. Chem. Phys.*, 2006, **8**, 1057-1065.
19. M. Wang, N. R. Jaegers, M.-S. Lee, C. Wan, J. Z. Hu, H. Shi, D. Mei, S. D. Burton, D. M. Camaioni, O. Y. Gutiérrez, V.-A. Glezakou, R. Rousseau, Y. Wang and J. A. Lercher, *J. Am. Chem. Soc.*, 2019, **141**, 3444-3455.
20. P. Liu, W. Hao and D. Mei, *J. Phys. Chem. C*, 2021, **125**, 15283-15291.
21. K. Stanciakova, B. Ensing, F. Göltl, R. E. Bulo and B. M. Weckhuysen, *ACS Catal.*, 2019, **9**, 5119-5135.
22. D. Mei and J. A. Lercher, *AIChE J.*, 2017, **63**, 172-184.
23. J. H. Hack, J. P. Dombrowski, X. Ma, Y. Chen, N. H. C. Lewis, W. B. Carpenter, C. Li, G. A. Voth, H. H. Kung and A. Tokmakoff, *J. Am. Chem. Soc.*, 2021, **143**, 10203-10213.
24. K. N. Han, S. Bernardi, L. Wang and D. J. Searles, *J. Phys. Chem. C*, 2017, **121**, 381-391.
25. C. J. Heard, L. Grajciar, C. M. Rice, S. M. Pugh, P. Nachtigall, S. E. Ashbrook and R. E. Morris, *Nat. Commun.*, 2019, **10**, 4690.
26. C. Tuma and J. Sauer, *Phys. Chem. Chem. Phys.*, 2006, **8**, 3955-3965.
27. S. F. Boys and F. Bernardi, *Mol. Phys.*, 1970, **19**, 553-566.
28. X. Huang, B. J. Braams and J. M. Bowman, *J. Chem. Phys.*, 2005, **122**.
29. E. Grifoni, G. Piccini, J. A. Lercher, V.-A. Glezakou, R. Rousseau and M. Parrinello, *Nat. Commun.*, 2021, **12**, 2630.
30. D. E. Resasco, S. P. Crossley, B. Wang and J. L. White, *Catal. Rev.*, 2021, **63**, 302-362.
31. Y. Xue, T. M. Sexton, J. Yang and G. S. Tschumper, *Phys. Chem. Chem. Phys.*, 2024, **26**, 12483-12494.
32. L. Ruiz Pestana, N. Mardirossian, M. Head-Gordon and T. Head-Gordon, *Chem. Sci.*, 2017, **8**, 3554-3565.
33. S. Eckstein, P. H. Hintermeier, R. Zhao, E. Baráth, H. Shi, Y. Liu and J. A. Lercher, *Angew. Chem. Int. Ed.*, 2019, **58**, 3450-3455.